

Kent-André Mardal

Finite Elements in Computational Mechanics

March 11, 2025

Springer Nature

Contents

1	A glimpse at the finite element method	3
1.1	Introduction	3
1.2	The finite element method in a nutshell	6
1.3	Brief remark on the strange world of partial differential equations and their discretizations	9
1.4	Further reading	11
1.5	Exercises	11
2	Crash course in Sobolev Spaces	13
2.1	Introduction	13
2.2	Norms, inner products and Sobolev spaces	13
2.3	Poincare's lemma	15
2.4	Spaces and sub-spaces, norms and semi-norms	16
2.5	Examples of Functions in Different Spaces	17
2.6	Sobolev Spaces and Polynomial Approximation	18
2.7	Eigenvalues and Finite Element Methods	19
2.8	Linear functionals and dual spaces	22
2.9	Negative and Fractional Norms	24
2.10	Boundary conditions, Traces and Fractional Sobolev Spaces	28
2.11	Exercises	29
3	Some common finite elements	31
3.1	Introduction	31
3.2	Some example finite elements: Lagrange and Hermite on the unit interval.	32
3.3	Mapping a reference element onto a physical element.	35

3.4	The connectivity of the mesh and the corresponding finite element space	36
3.5	Exercises	37
4	The finite element method for elliptic problems	39
4.1	The weak formulation and the finite element formulation	39
4.2	What is an elliptic equation ?	41
4.3	An <i>a priori</i> Error Estimate	42
4.4	Exercises	45
5	Discretization of a convection-diffusion problem	47
5.1	Introduction	47
5.2	Streamline diffusion/Petrov-Galerkin methods	52
5.3	Well posedness of the continuous problem	55
5.4	Error estimates	58
5.5	Exercises	59
6	Stokes problem	61
6.1	Introduction	61
6.2	Finite Element formulation	64
6.3	Examples of elements	68
6.4	Stabilization techniques to circumvent the Babuska-Brezzi condition	70
6.5	Exercises	71
7	Efficient Solution Algorithms: Iterative methods and Preconditioning	73
7.1	The simplest iterative method: the Richardson iteration	74
7.2	The idea of preconditioning	80
7.3	Krylov methods and preconditioning	82
7.4	Exercises	92
8	Linear elasticity and singular problems	97
8.1	Introduction	97
8.2	The operator $\nabla \cdot \epsilon$ and rigid motions	99
8.3	Locking	104
9	Alternative Formulations	109
9.1	Introduction	109
9.2	Least square formulation of primal formulation	110
9.3	The Mixed formulation	111

Contents	vii
Index	113
References	115

Not included

- Hdiv, Hcurl elements
- $\text{frac}(A)$ observation
- time-discretization
- least squares
- adjoint

Things deliberately not shown in the book, but left as exercises.

- Definition of norms, inner products and shown that Sobolev norms, inner products actually defines norms and inner products
- Equivalence between semi-norms and norms, given Poincare.

Chapter 1

A glimpse at the finite element method

1.1 Introduction

As a starting point for the finite element method, let us consider the mother problem of partial differential equations, the elliptic problem: Find the solution u of the problem

$$-\nabla \cdot (k \nabla u) = f \quad \text{in } \Omega, \quad (1.1)$$

$$u = g \quad \text{on } \partial\Omega_D, \quad (1.2)$$

$$k \frac{\partial u}{\partial n} = h \quad \text{on } \partial\Omega_N. \quad (1.3)$$

We include here both Dirichlet (1.2) and Neumann (1.3) boundary conditions and assume $\partial\Omega = \partial\Omega_D \cup \partial\Omega_N$ and $\partial\Omega_D \cap \partial\Omega_N = \emptyset$.

Solving this problem *properly* for general Ω, f, g, h , is not an easy task, but is still routinely done computationally everyday in a variety of applications in science and engineering. Our method of choice in this book is the finite element method - a practical, versatile and efficient method that also allows for rigorous error control and detailed analysis. However, unusual concepts like weak or variational formulations, trial and test functions, Sobolev spaces etc. show up in the finite element methods and many find them troublesome and strange. To motivate these concepts we start with some "philosophical" considerations that lead to three challenges which will be resolved by the finite element method. The first challenge: the above equation is the so-called strong formulation and its interpretation is (directly) that:

For every point $x \in \Omega$ the equation

$$-\nabla \cdot (k(x)\nabla u(x)) = f(x), \quad (1.4)$$

should be valid. Hence, u, f are functions and if we assume that f is a continuous function then u is continuous with two derivatives that are also continuous. More formally, $f \in C(\Omega)$ directly leads to the requirement that $u \in C^2(\Omega)$. In general it is however well known, and we will meet many such solutions in this course, that $u \notin C^2(\Omega)$ are also solutions to (1.1).

In this book, it will be central to compare differential operators with matrices in order to build intuition. So, let us assume that (1.4) is somehow (ignoring the boundary conditions for now) represented as a linear system, i.e.,

$$Au = b. \quad (1.5)$$

This leads us to our second challenge: In order to have a linear system with a well-defined solution we at least need the same number of equations and unknowns, ie. A is a $\mathbb{R}^{N \times N}$ matrix and u, f are vectors in \mathbb{R}^N . How can we make numerical methods that ensure the same number of equations and unknowns? There are infinitely many points in any continuous domain. Is it the same number of unknowns in (1.4)?

A direct comparison of (1.4) and (1.5) would for instance be to assume that i 'th equation of $Au = b$ correspond to the point x_i in (1.4). Hence, $\sum_j A_{ij}u_j = b_i$ corresponds to $-\nabla \cdot (k(x_i)\nabla u(x_i)) = f(x_i)$ for a set of points $\{x_1, \dots, x_n\}$. Then the number of equations (or number of rows in A) is N and equals the number of points in the discrete domain. Assuming for instance that Ω is the unit square with n internal points (as the boundary is currently ignored) in both the x - and y -direction gives that $N = n^2$. With a slight abuse of notation¹, we may then enumerate the points as $x_i = (x_j, y_k)$ where $i = j(N-1) + k$ for $j, k \in (1, N)$. In order to get a non-singular matrix, the number of unknowns should equal the number of equations. We do obtain N unknowns if we assume that for every point in the domain we have an unknown $u_k = u(x_i, y_j)$, $k = j + i(N-1)$ corresponding to the equations $-\nabla \cdot (k\nabla u(x_i, y_j)) = f(x_i, y_j)$. It is however not clear how to make sense of u outside the points (x_i, y_j) . Furthermore, an obvious mathematical question is then to what extent we recover $u \in C^2(\Omega), f \in C(\Omega)$ as n tends to ∞ with this construction. In general, we will not recover the conditions set by the strong formulation,

¹ We avoid bold face notation for coordinates.

although a proper mathematical explanation of this is beyond the scope of this book. The reader is referred to [7] for a more detailed explanation of the strong formulation.

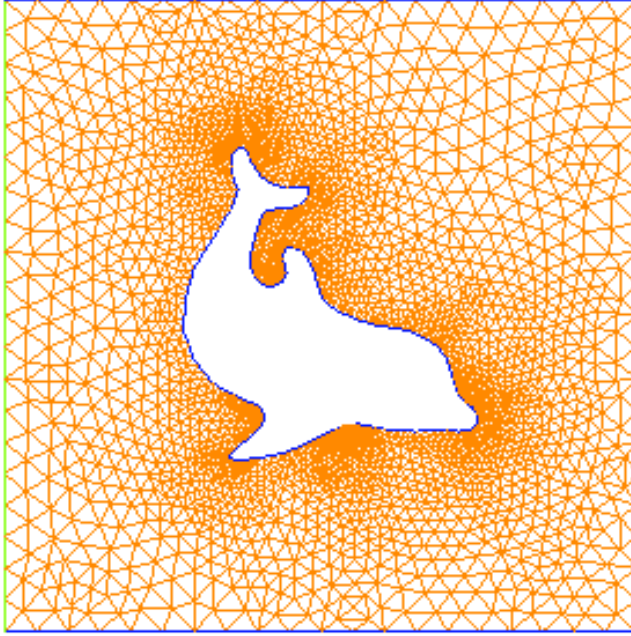


Fig. 1.1 An example mesh of a swimming dolphin.

Computationally, we need to resort to finite resolutions and this brings us to our third challenge. In Figure 1.1 we see triangulation of domain outside the drawing of a swimming dolphin. We can immediately see that it will be difficult to formulate a finite difference approach on this domain as the nodal points does not form squares. Hence, a stencil like:

$$\frac{u(x+h, y) + u(x, y+h) - 4u(x, y) + u(x-h, y) + u(x, y-h)}{h^2} (\approx \Delta u)$$

will not be able to exploit the triangulation. Furthermore, the stencil will cross $\partial\Omega$.

1.2 The finite element method in a nutshell

The finite element method (FEM) resolves these three challenges by combining 1) the so-called weak formulations which reduces the demands of differentiability of the solution with 2) trial and test functions constructed by the same approach leads to $N \times N$ matrices and 3) a structured approach of integration adjusted to the underlying meshes.

Hence, before we start with FEM, let us recap some fundamental results of calculus that will lead to the weak formulation, *the Gauss-Green's lemma*:

$$\int_{\Omega} -\nabla \cdot (k \nabla u) v \, dx = \int_{\Omega} (k \nabla u) \cdot \nabla v \, dx - \int_{\partial \Omega} k \frac{\partial u}{\partial n} v \, ds. \quad (1.6)$$

Here, we have two functions u and v . We will in the following refer to them as the trial function and the test function, respectively. We note that we are able to move derivatives from u to v and hence reduce the strict requirement of $u \in C^2(\Omega)$ by a compensating requirement for v .

Next, we apply the boundary conditions. That is, for the Dirichlet condition (1.2) we already know that $u = g$. Hence, u is not an unknown on that part of the boundary. Therefore, we may let $v = 0$ at $\partial \Omega_D$ and simply remove the associated equations at that part of the boundary. Further, by inserting the Neumann condition, we obtain that

$$\int_{\partial \Omega} k \frac{\partial u}{\partial n} v \, ds = \int_{\partial \Omega_D} k \frac{\partial u}{\partial n} v \, ds + \int_{\partial \Omega_N} k \frac{\partial u}{\partial n} v \, ds \quad (1.7)$$

$$= \int_{\partial \Omega_D} k \frac{\partial u}{\partial n} 0 + \int_{\partial \Omega_N} h v \, ds \quad (1.8)$$

As such we arrive at the *weak formulation* of the elliptic problem: Find u such that

$$\int_{\Omega} k \nabla u \cdot \nabla v \, dx = \int_{\Omega} f v \, dx + \int_{\Omega_N} h v \, ds, \quad \forall v \quad (1.9)$$

Here, we assume as mentioned that $u = g$ and $v = 0$ on $\partial \Omega_D$. We will come back to what $\forall v$ means in a more precise sense later.

At this point we *summarize how to obtain a weak formulation* as this will be done over and over again throughout this book. First, we multiply with a test function and integrate. Second, the Gauss-Green lemma (or a similar lemma) is applied and third we apply the boundary conditions.

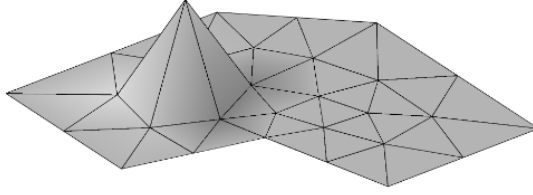


Fig. 1.2 One finite element basis function /pyramide function associated with a particular node.

Remark 1.1 We remark that the test function v plays the role of pointwise evaluation in the strong formulation (1.4). That is, we evaluate (or test) the above equation with respect to many different test functions, which in the previous formulation corresponded to many different points. We notice that if the test functions are Dirac delta, δ^2 , functions then we recover the strong formulation. However, since but we cannot differentiate the δ functions (in a classical sense) we are only able to evaluate the left-hand side of (1.6). Using the δ functions as test functions and avoiding the use of Gauss-Green is often called the *collocation method* and is used e.g. by the Runge-Kutta method. However, it is seldom used for FEM because of the high demands on the differentiability on u .

The second challenge was to find formulations that lead to linear systems with $N \times N$ matrices. The finite element method resolves this challenge by employing the same basis functions for both the trial and the test functions. That is, let the trial and test functions be as follows:

$$u = \sum_{j=1}^N u_j N_j \quad \text{and} \quad v = N_i, \quad i = 1 \dots N. \quad (1.10)$$

Here $\{N_i\}$ is a set of basis functions that needs to be chosen somehow. Choosing the same basis functions for the trial and test functions, as above, is referred to as the Galerkin method.

Furthermore, as the third challenge above mentioned, the basis functions needs to adapt to a mesh. There are many possibilities and one may target the

² The Dirac function associated with $x = 0$, δ_0 , is such that $\int_{-\infty}^{\infty} \delta_0 dx = 1$; $\delta_0(x) = 0, \forall x \neq 0$; and $\delta_0(0) = \infty$.

basis function to the problem at hand. The simplest basis function is shown in Fig 1.2. Here, the basis function is chosen as linear functions / pyramids associated with the nodal points, so-called Lagrange element of first order. There are many, many different finite element functions to choose from and they have different properties. Lists of common and unusual elements available in FEniCS can be found in [11].

The FEM problem is obtained by inserting (1.10) into the weak formulation (1.9), i.e.

$$\int_{\Omega} k \nabla \sum_j u_j N_j \cdot \nabla N_i dx = \int_{\Omega} f N_i dx + \int_{\Omega_N} h N_i ds \quad \forall j.$$

We pull the summation out:

$$\sum_j u_j \int_{\Omega} k \nabla N_j \cdot \nabla N_i dx = \int_{\Omega} f N_i dx + \int_{\Omega_N} h N_i ds \quad \forall j.$$

Hence, with

$$A_{ij} = \int_{\Omega} k \nabla N_j \cdot \nabla N_i dx,$$

$$b_i = \int_{\Omega} f N_i dx + \int_{\Omega_N} h N_i ds$$

we arrive at the following linear system

$$Au = b$$

We remark here that for the matrix entries $\{A_{ij}\}$ the trial function dictates the row-wise numbering whereas the test functions dictate the column-wise numbering. Usually, the same numbering strategy is used for both and since both the trial and test spaces consists of N basis functions as above, we obtain an $N \times N$ matrix. Furthermore, the matrix will be symmetric if the underlying equations are.

The following code solves the Poisson problem on the unit square consisting of 32×32 rectangles, where each rectangle is divided in two and $f = 1$, $g = 0$ and $h = x$. Dirichlet conditions are set for $y = 0$ and Neumann for the rest of $\partial\Omega$.

```
from dolfin import *
```

```

# Create mesh and define function space
mesh = UnitSquareMesh(32, 32)
V = FunctionSpace(mesh, "Lagrange", 1)

# Define Dirichlet boundary (x = 0 or x = 1)
def boundary(x): return x[0] < DOLFIN_EPS

# Define boundary condition
u0 = Constant(0.0)
bc = DirichletBC(V, g, boundary)

# Define variational problem
u = TrialFunction(V)
v = TestFunction(V)
f = Constant(1)
g = Expression("x[0]")
a = inner(grad(u), grad(v))*dx
L = f*v*dx + h*v*ds

# Compute solution
u = Function(V)
solve(a == L, u, bc)

# Save solution in VTK format
file = File("poisson.pvd")
file << u

```

1.3 Brief remark on the strange world of partial differential equations and their discretizations

A fundamental property in both the theory of partial differential equations and numerical analysis is the concept of well-posedness. In Hadamard's definition a problem is well-posed if three conditions are met for the given input. The solution 1) exists, is 2) unique and 3) depends continuously on the input. Hence, if we have two inputs to our problem, b_1 and b_2 and unique solutions u_1 and u_2 constructed such that $Au_1 = b_1$ and $Au_2 = b_2$, then the difference between u_1 and u_2 should be bounded by the differences between b_1 and b_2 . In terms of linear algebra, we directly obtain well-posedness if A is a non-singular matrix. That is, we directly obtain

$$A(u_1 - u_2) = (b_1 - b_2)$$

which leads to

$$\|(u_1 - u_2)\| = \|A^{-1}(b_1 - b_2)\| \leq \|A^{-1}\| \|b_1 - b_2\|$$

and

$$\|(b_1 - b_2)\| = \|A(u_1 - u_2)\| \leq \|A\| \|u_1 - u_2\|$$

Hence, the difference between the solutions u_1 and u_2 in the sense $\|u_1 - u_2\|$ is bounded continuously both above and below by the difference in data in the sense $\|b_1 - b_2\|$. In the above, the norms have not been specified, but then, in a finite dimensional setting, all vector norms are equivalent. These rather simple observations on the linear algebra level does not easily extend to the continuous setting of partial differential equations. For instance, for Poisson problems with homogenous Dirichlet conditions but different source terms f_1 and f_2 the unique solutions u_1 and u_2 constructed such that $-\Delta u_1 = f_1$ and $-\Delta u_2 = f_2$, we expect by an direct analog of the linear algebra considerations above that

$$\|u_1 - u_2\| \leq \|(-\Delta)^{-1}\| \|f_1 - f_2\|$$

In contrast to the finite dimensional case, we really need to be careful with our choice of norms here. In fact, the norm we will be using later on is more related to the square root of the matrix or operator. We will make it more precise later, but let us remark that if

$$Au = b$$

and we are able to compute the square root of the matrix A then we also have directly by multiplying with $A^{-1/2}$ on both sides:

$$A^{1/2}u = A^{-1/2}b$$

Then, as we will see, the notion

$$\|A^{1/2}(u_1 - u_2)\| = \|A^{-1/2}(b_1 - b_2)\|$$

is what gives us precise estimates in a wide range of situations.

We remark that $\Delta = \nabla \cdot \nabla$ and as such ∇ can be interpreted as a square root of Δ . There are however some difficulties that arise with this notion. Let us consider the problem in 1D, using FDM. The stencil is then

$$-u_{xx} \approx Au = \frac{-u_{i+1} + 2u_i - u_{i-1}}{h^2},$$

where $u_i = u(x_i)$ and $x_i = ih$, $i = 0, \dots, N$. For a mesh with two internal degrees of freedom, the corresponding matrix is

$$A = \frac{1}{h^2} \begin{pmatrix} 2 & -1 \\ -1 & 2 \end{pmatrix}$$

Let B

$$Bu = \frac{1}{h} \begin{pmatrix} 1 & -1 & 0 \\ 0 & 1 & -1 \end{pmatrix}$$

Obviously,

$$A = B^T B$$

However, B is not unique. Furthermore, it is a rectangular matrix that makes it difficult to invert it. In particular, it has a one-dimensional kernel consisting of the constant vector $c(1, 1, 1)^T$, where $c \in \mathbb{R}$. Likewise in the continuous setting ∇ has a kernel of constant functions. However, and withough any mathematical rigour, the correct and actually quite practical variant of the above estimate is

$$\|\nabla(u_1 - u_2)\| = \|\nabla^{-1}(f_1 - f_2)\|$$

We do however need to make sense of the ∇^{-1} . For now it is enough to think of it as some form of antiderivative. Here, for instance u_1, f_1 may be the actual continuous solution and input data whereas the u_2, f_2 are the numerical solution and input data.

1.4 Further reading

There are several excellent and highly recommended books on the finite element method [2, 3].

1.5 Exercises

Exercise 1.1 Consider the problem $-u''(x) = x^2$ on the unit interval with $u(0) = u(1) = 0$. Let $u = \sum_{k=1}^N u_k \sin(\pi kx)$ and $v = \sin(\pi lx)$ for $l = 1, \dots, N$, for e.g. $N = 10, 20, 40$. and solve (1.9). What is the error in L_2 and L_∞ .

Exercise 1.2 Consider the same problem as in the previous exercise, but using Bernstein polynomials. That is, the basis for the Bernstein polynomial of order N on the unit interval is $B_k(x) = x^k(1-x)^{N-k}$ for $k = 0, \dots, N$. Let $u = \sum_{k=0}^N u_k B_k(x)$ and $v = B_l(x)$ for $l = 0, \dots, N$ and solve (1.9). What is the error in L_2 and L_∞ in terms of N for $N = 1, 2, \dots, 10$. Remark: Do the basis functions satisfy the boundary conditions? Should some of them be removed?

Exercise 1.3 Consider the same problem as in the previous exercise, but with $-u''(x) = \sin(k\pi x)$ for $k = 1$ and $k = 10$.

Exercise 1.4 Consider the same problem as in the previous exercise, but with the finite element method in for example FEniCS, FEniCSx or Firedrake, using Lagrange method of order 1, 2 and 3.

Chapter 2

Crash course in Sobolev Spaces

2.1 Introduction

Sobolev spaces are fundamental in the analysis of partial differential equations and also for finite element methods. Many books provide a detailed and comprehensive analysis of these spaces that in themselves deserve significant attention if one wishes to understand the foundation that the analysis of partial differential equations relies on. In this chapter we will however not provide a comprehensive mathematical description of these spaces, but rather try to provide insight into their use.

We will here provide the definition of these spaces. Further we will show typical functions, useful for finite element methods, that are in some but not all spaces. We also show how different norms capture different characteristics.

2.2 Norms, inner products and Sobolev spaces

Function spaces are vector spaces where the vectors are functions. Obviously, this makes sense as functions can be added to each other, multiplied with scalars etc., so all requirements for a vector space can be easily verified.

We will use L^p spaces which are defined as follows. Let u be a scalar valued function on the domain Ω , which for the moment will be assumed to be the unit interval $(0, 1)$. Then the L^p norm on Ω is:

$$\|u\|_p = \left(\int_0^1 |u|^p dx \right)^{1/p}.$$

$L^p(\Omega)$ consists of all functions for which $\|u\|_p < \infty$. Sobolev spaces generalize L^p spaces by also including the derivatives. On the unit interval, the $W^{k,p}$ norm is defined as

$$\|u\|_{k,p} = \left(\int_{\Omega} \sum_{i \leq k} \left| \frac{\partial^i u}{\partial x^i} \right|^p dx \right)^{1/p}. \quad (2.1)$$

Then the Sobolev space $W^{k,p}(\Omega)$ consists of all functions with $\|u\|_{k,p} < \infty$. $W^{k,p}$ is a so-called Banach space - that is a complete¹ normed vector space. Notice that the derivative is defined *weakly*, ie. in the sense that existence is required only in L^p . For instance, a function may have derivatives that are infinite on zero measures, such as point-wise infinities.

The corresponding semi-norm, which only include the highest order derivative is

$$|u|_{k,p} = \left(\int_{\Omega} \left| \frac{\partial^k u}{\partial x^k} \right|^p dx \right)^{1/p}. \quad (2.2)$$

The case $p = 2$ is special in the sense that not only a norm is defined but also an inner product. The Banach space then forms a Hilbert space and these named with H in Hilbert's honor. That is $H^k(\Omega) = W^{k,2}(\Omega)$. The inner product between the functions u and v is:

$$(u, v)_k = \sum_{i \leq k} \int_{\Omega} \frac{\partial^i u}{\partial x^i} \frac{\partial^i v}{\partial x^i} dx.$$

For the most part, we will employ the two spaces $L^2(\Omega)$ and $H^1(\Omega)$, but also other spaces will be used from time to time. The difference between the norm in $L^2(\Omega)$ and $H^1(\Omega)$ is illustrated in the following example.

KAM: Need an example env easier to reference to.

Example Norms of $\sin(k\pi x)$. Consider the functions $u_k = \sin(k\pi x)$ on the unit interval. The norms of u_k are shown in Table 2.1, while Fig. 2.1 shows the function for $k = 1$ and $k = 10$. Clearly, the L^2 and L^7 behave similarly in the sense that they remain the same as k increases. On the other hand, the

¹ We will not go into the details of complete spaces in this book, but remark that the space of real numbers is complete, while the space of rational numbers is not.

H^1 norm of u_k increases dramatically as k increases. The following code shows how the norms are computed using FEniCS.

```
from dolfin import *

N = 10000
mesh = UnitInterval(N)
V = FunctionSpace(mesh, "Lagrange", 1)

for k in [1, 100]:
    u_ex = Expression("sin(k*pi*x[0])", k=k)
    u = project(u_ex, V)

    L2_norm = sqrt(assemble(u**2*dx))
    print "L2 norm of sin(%d pi x) %e" % (k, L2_norm)

    L7_norm = pow(assemble(abs(u)**7*dx), 1.0/7)
    print "L7 norm of sin(%d pi x) %e" % (k, L7_norm)

    H1_norm = sqrt(assemble(u*u*dx+inner(grad(u), grad(u))*dx))
    print "H1 norm of sin(%d pi x) %e" % (k, H1_norm)
```

$k \backslash \text{norm}$	L^2	L^7	H^1
1	0.71	0.84	2.3
10	0.71	0.84	22
100	0.71	0.84	222

Table 2.1 The L^2 , L^7 , and H^1 norms of $\sin(k\pi x)$ for $k = 1, 10, 100$.

2.3 Poincare's lemma

Poincare's inequality states that for $u \in H_{0,D}^1(\Omega)$ we have

$$\|u\|_{L^2(\Omega)} \leq C \|\nabla u\|_{L^2(\Omega)} \quad (2.3)$$

We will not prove this inequality in this book (see e.g. [7]), but we note that it can be motivated by considering the Taylor series approximation. From basic calculus we know that:

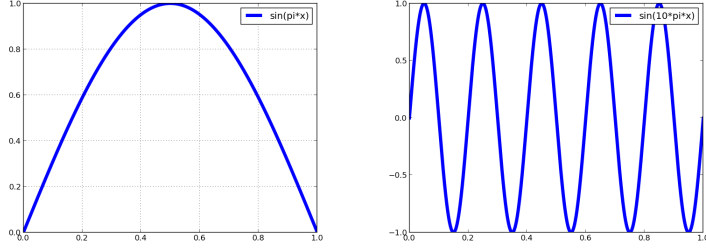


Fig. 2.1 Left picture shows $\sin(\pi x)$ on the unit interval, while the right picture shows $\sin(10\pi x)$.

$$|f(x+h)| \leq |f(x)| + h \max_{x \leq x^* \leq x+h} |f'(x^*)|$$

Choosing x on $\partial\Omega_D$ makes $f(x) = 0$ and hence $f(x+h)$ can be bounded by the derivative of f . Of course, Poincare's result provides a bounds on the integral rather than the pointwise sense of Taylor, but the results are similar.

2.4 Spaces and sub-spaces, norms and semi-norms

The Sobolev space with k derivatives in $L_2(\Omega)$ was denoted by $H^k(\Omega)$. The subspace of H^k with $k-1$ derivatives equal to zero at the boundary is denoted $H_0^k(\Omega)$. For example, $H_0^1(\Omega)$ consists of all functions in H^1 that are zero at the boundary. Similarly, we may also defined a subspace $H_g^1(\Omega)$ which consists of all functions in $H^1(\Omega)$ that are equal to the function g on the boundary.

The norm $\|\cdot\|_{p,k}$ defined in (2.1) is a norm which means that $\|u\|_{p,k} > 0$ for all $u \neq 0$. On the other hand $|\cdot|_{p,k}$ is a semi-norm, meaning that $|u|_{p,k} \geq 0$ for all u . The space $H^1(\Omega)$ is defined by the norm

$$\|u\|_1 = \|u\|_{H^1} = \left(\int_{\Omega} u^2 + (\nabla u)^2 dx \right)^{1/2}$$

and contains all functions for which $\|u\|_1 \leq \infty$. The space has an associated inner product. Let $u, v \in H^1(\Omega)$ then the inner product is

$$(u, v)_1 = (u, v)_{H^1} = \int_{\Omega} uv + \nabla u \nabla v \, dx.$$

The corresponding semi-norm $|\cdot|_1$ defined as

$$|u|_1 = \|u\|_{H_0^1} = \left(\int_{\Omega} (\nabla u)^2 \, dx \right)^{1/2}$$

We will see later that Poincaré's lemma ensures that $\|\cdot\|_1$ and $|\cdot|_1$ are equivalent norms on the subspace H_0^1 (see Exercise 4.3). On H_0^1 we have the associated inner product

$$(u, v)_{H_0^1} = \int_{\Omega} \nabla u \nabla v \, dx.$$

2.5 Examples of Functions in Different Spaces

The above functions $\sin(k\pi x)$ are smooth functions that for any k are infinitely many times differentiable. They are therefore members of any Sobolev space as long as Ω is bounded.

On the other hand, the step function in upper picture in Figure 2.2 is discontinuous in $x = 0.2$ and $x = 0.4$. Obviously, the function is in $L^2(0, 1)$, but the function is not in $H^1(0, 1)$ since the derivative of the function consists of Dirac's delta functions $\delta_{0.2}$ and $-\delta_{0.4}$ that are ∞ at $x = 0.2$ and $-\infty$ in $x = 0.4$ ².

The hat function in the lower picture in Figure 2.2 is a typical first order finite element function. The function is in both $L^2(0, 1)$ and $H^1(0, 1)$ (see Exercise 2.5). In general, functions in $H^q(0, 1)$ are required to be in $C^{q-1}(0, 1)$, where $C^k(0, 1)$ is the class where the k 'th derivatives exist and are continuous on the unit interval.

Remark 2.1 In $C^k(\Omega)$ a function and its k derivatives can be evaluated at any given point in Ω and the result will be a finite value. How about functions in $H^k(\Omega)$? In general only functions in $H^k(\Omega)$ for $k \geq 2$ allow pointwise evaluation. The exact relationship between continuous functions and Sobolev spaces are covered by the Sobolev Embedding Theorem [7], which will not be

² We remark that for $y \in \Omega$ $\int_{\Omega} \delta_y \, dx = 1$ However, $\int_{\Omega} \delta_y^2 \, dx = \infty$.

covered in this book. Anyways, in $L^2(\Omega)$ or $H^1(\Omega)$ we should make note and be careful when we perform pointwise evaluations.

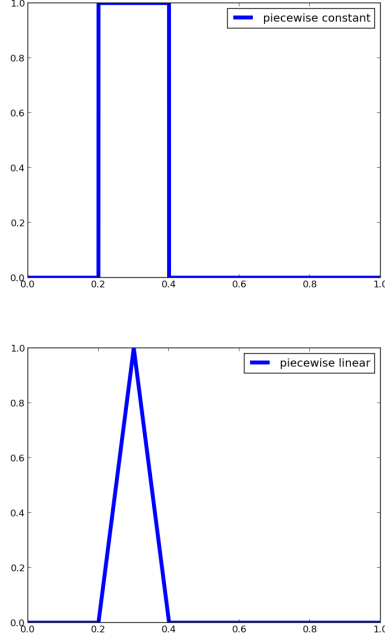


Fig. 2.2 The upper picture shows a piecewise function, discontinuous at $x = 0.2$ and $x = 0.4$, while the lower picture shows a linear function that is continuous.

2.6 Sobolev Spaces and Polynomial Approximation

From Taylor series approximation we know that $f(x+h)$ may be approximated by $f(x)$ and a polynomial in h that depends on the derivatives of f . To be precise,

$$|f(x+h) - P_{h,k}f(x)| \leq \mathcal{O}(h^{k+1}).$$

Here, $P_{h,k}f(x)$ is the following polynomial of degree k in h ,

$$P_{h,k}f(x) = f(x) + \sum_{n=1}^k \frac{f^{(n)}(x)}{n!} h^n.$$

where $f^{(n)}$ denotes the n 'th derivative of f .

In general, approximation by Taylor series bears strong requirement on the smoothness of the solution which needs to be differentiable in a point-wise sense. Hence, we need to defined the polynomials in an alternative way, but the results are similar. We conclude, without proof, that in Sobolev spaces we have the very useful approximation property

$$|u - P_m u|_{k,p} \leq Ch^{m-k} |u|_{m,p} \quad \text{for } k = 0, \dots, m \text{ and } p \geq 1. \quad (2.4)$$

This property is used extensively in analysis of finite element methods and is called the Bramble-Hilbert lemma for $k \geq 2$. The case $k = 1$ was included by a special interpolation operator by Clement, the so-called Clement interpolant. For proof, see e.g. [2, 3]. In Chapter 3, Example 3.2.1 we will consider an explicit construction (the Lagrange interpolation) in more detail.

2.7 Eigenvalues and Finite Element Methods

Eigenvalues and eigenvectors are enormously useful for understanding the properties of matrices and operators. Let us therefore consider how to compute these when using the finite element method.

It is well known that for $-\Delta$ with homogenous Dirichlet conditions on the unit interval $(0, 1)$, the eigenvalues and eigenvectors are $(\pi k)^2$ and $\sin(\pi k x)$, $k = 1, \dots, \infty$, respectively. It is natural to expect that the eigenvalues in the discrete setting approximate the continuous eigenvalues such that the minimal eigenvalue is $\approx \pi^2$, while the maximal eigenvalue is $\approx \pi^2/h^2$, where $k = 1/h$ corresponds to the highest frequency that may be represented on a mesh with element size h . Computing the eigenvalues of the finite element stiffness matrix in FEniCS as³,

³ We use the `assemble_system` function to enforce the Dirichlet condition in symmetric fashion.

```
A = assemble_system(inner(grad(u), grad(v))*dx, Constant(0)*v*
                    dx, bc)
```

reveals that the eigenvalues are differently scaled. In fact, the minimal eigenvalue is $\approx \pi^2 h$ and that the maximal eigenvalue is $\approx \pi^2/h$, see Fig.2.3 (red and blue curves). The reason is that the finite element method introduces a mesh-dependent scaling due to the fact that it is a variational method. Specifically, if we want to approximate a f as $\sum_j f_j N_j$ we notice that we should calculate f_j in a variational sense as follows:

$$\sum_j \int_{\Omega} f_j N_j N_i dx = \int_{\Omega} f N_i dx.$$

Hence, we notice here that, we are solving a linear system

$$Mf = b, \text{ with } M_{ij} = \int_{\Omega} N_j N_i dx \text{ and } b_i = \int_{\Omega} f N_i dx$$

Both $\{f_i\}_i$ and $\{b_i\}_i$ are *representations* of f , often called the *nodal* and *dual* representations [13]. They scale differently since the entries of the mass matrix scale with the size of the elements in the mesh.

To estimate the continuous eigenvalues, we need to make sure that both the left- and right-hand sides are in the same representation, either nodal or dual. Hence, for a nodal representation of the eigenvalues and eigenvectors, we should consider the generalized eigenvalue problem,

$$Ax = \lambda Mx, \tag{2.5}$$

where A is the above mentioned stiffness matrix and M is the mass matrix (or the finite element identity matrix)

```
M = assemble_system(inner(u*v*dx, Constant(0)*v*dx, bc)
```

Figure 2.5 shows the eigenvalues of $-\Delta$, A , and (2.5) based on the following code:

```
from dolfin import *
import numpy
from scipy import linalg, matrix

def boundary(x, on_boundary): return on_boundary

for N in [100, 1000]:
    mesh = UnitIntervalMesh(N)
```

```

V = FunctionSpace(mesh, "Lagrange", 1)
u = TrialFunction(V)
v = TestFunction(V)

bc = DirichletBC(V, Constant(0), boundary)
A, _ = assemble_system(inner(grad(u), grad(v))*dx, Constant(
    0)*v*dx, bc)
M, _ = assemble_system(u*v*dx, Constant(0)*v*dx, bc)

AA = matrix(A.array())
MM = matrix(M.array())

k = numpy.arange(1, N, 1)
eig = pi**2*k**2

l1, v = linalg.eigh(AA)
l2, v = linalg.eigh(AA, MM)

print "l1 min, max ", min(l1), max(l1)
print "l2 min, max ", min(l2), max(l2)
print "eig min, max ", min(eig), max(eig)

import pylab
pylab.loglog(l1[2:], linewidth=5) # exclude Dirichlet values
pylab.loglog(l2[2:], linewidth=5) # exclude again
pylab.loglog(eig, linewidth=5)
pylab.legend(["eig(A)", "eig(A,M)", "cont. eig"], loc="upper
    left")

pylab.show()

```

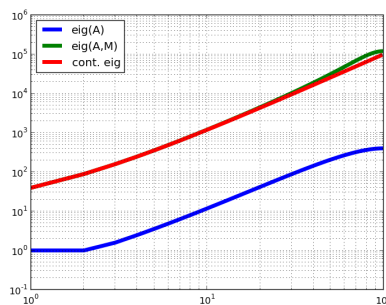


Fig. 2.3 A log-log plot of the eigenvalues of A , $M^{-1}A$, and $-\Delta$.

From Figure 2.3 we see that the eigenvalues of (2.5) and $-\Delta$ are close, while the eigenvalues of A is differently scaled. We remark that we excluded the two smallest eigenvalues in the discretized problems as they correspond to the Dirichlet conditions.

2.8 Linear functionals and dual spaces

A functional on a vector space V is an object $L(\cdot)$ that when given a vector $v \in V$, returns a real number. For example let $V = \mathbb{R}^n$ and the inner-product in use be the l_2 inner product, ie. $(x, y)_{l_2} = \sum_i x_i y_i$. Then any vector $z \in \mathbb{R}^n$ together with l_2 inner product forms a linear functional on V as

$$L_z(x) = (z, x)_{l_2}.$$

It is easy to verify that L_z is linear and bounded.

By choosing z appropriately we may define linear functionals that for example 1) returns the i 'th component of the vector, i.e. by letting $z = e_i$ where e_i is the i 'th unit vector or 2) computes the sum of a vector, i.e. by letting $z = (1, \dots, 1)$. The mentioned functionals 1) and 2) are linear, but examples of non-linear functionals may e.g. be sums of powers of the components, ie.

$$L_p(v) = \sum_i v_i^p.$$

The dual space of V , written as V^* , is the space of all linear functionals on V . To define we need the definition of the dual norm.

Definition The dual norm and the corresponding dual space.

Let $(\cdot, \cdot)_V$ be an inner product over the Hilbert space V and let $f(\cdot)$ be a linear functional on V . The dual norm of f is

$$\|f\|_{V^*} = \sup_{v \in V} \frac{f(v)}{\sqrt{(v, v)_V}}.$$

The space V^* consists of all f such that $\|f\|_{V^*} < \infty$. □

We remark that the dual space of \mathbb{R}^n is \mathbb{R}^n , ie. $(\mathbb{R}^n)^* = \mathbb{R}^n$. In general however, the dual space V^* may in general be different from V .

Functionals on function spaces are analogous to functionals on \mathbb{R}^n . For example, the example functionals 1) and 2) above directly maps to corresponding

functionals on function spaces with the l_2 inner product replaced by the $L^2(\Omega)$ inner product. That is, for example the counter-part of example 1) above, the i 'th component of a vector, is function evaluation in a point x_i . The corresponding functional is:

$$L_1(u) = \int_{\Omega} u(x) \delta_{x_i}(x) dx,$$

with δ_{x_i} being the Dirac delta function associated with x_i . Similarly, the example 2) the summation of all entries in a vector simply corresponds to the integral of the function

$$L_2(u) = \int_{\Omega} u(x) dx.$$

We notice immediately that the situation is more complicated for function spaces than for \mathbb{R}^n . There are obviously functions in which pointwise evaluation and/or integrals are not well defined. Consider for example the function $f(x) = x^\alpha$. Clearly, if $\alpha < 0$ then $f(0) = \infty$. Furthermore, if $\alpha \geq 0$ and our domain of interest is \mathbb{R}^+ then

$$\int_0^\infty f(x) dx = \infty.$$

Hence, which linear functionals that belongs to which dual spaces are not always easy to grasp and may require careful considerations. Let us for example, consider the one-dimensional function space V spanned by x^α and associated with the L^2 inner product. Then clearly, $g(x) = x^\beta$ and the associated linear functional $L_g(\cdot)$ is in V^* if $\alpha + \beta < -1$ since

$$L_g(f) = \int_0^\infty f(x)g(x) dx < \infty$$

The dual space of H_0^1 with respect to the L^2 inner product is commonly referred to as H^{-1} . Formally, by using the above definition, its norm is

$$\|f\|_{-1} = \sup_{v \in H_0^1} \frac{f(v)}{|v|_1}.$$

Clearly, the $H^{-1} \subset L^2$, using the inequalities of Cauchy–Schwarz and Poincaré, see Sec. 2.3, since

$$\|f\|_{-1} = \sup_{v \in H_0^1} \frac{f(v)}{|v|_1} = \sup_{v \in H_0^1} \frac{\int_{\Omega} f v dx}{\sqrt{\int_{\Omega} (\nabla v)^2 dx}} \leq \sup_{v \in H_0^1} \frac{\|f\|_0 \|v\|_0}{|v|_1} \leq C \|f\|_0$$

In fact, $H_0^1(\Omega) \subset L^2(\Omega) \subset H^{-1}(\Omega)$.

A major result in functional analysis, the *Riesz representation theorem*, states that if V is a Hilbert space with the inner product $(\cdot, \cdot)_V$ then for every $f \in V^*$ there is a corresponding $u \in V$ such that

$$(u, v)_V = f(v), \quad \forall v \in V.$$

Furthermore,

$$\|u\|_V = \|f\|_{V^*}.$$

2.9 Negative and Fractional Norms

As will be discussed more thoroughly later, $-\Delta$ is a symmetric positive operator on H_0^1 and can be thought of as an infinite dimensional matrix that is symmetric and positive. Indeed, in the concrete case of $\Omega = (0, 1)$, in Sec. 2.7 we discussed the spectral decomposition of $-\Delta$ in the continuous case along with the corresponding discretization using finite elements. Let us exploit the spectral decomposition of $-\Delta$ to make sense of negative, fractional and dual norms in the simple example where we have special decomposition.

It is also known from Riesz representation theorem that if u solves the problem

$$\begin{aligned} -\Delta u &= f, & \text{in } \Omega, \\ u &= 0, & \text{on } \partial\Omega \end{aligned}$$

then

$$|u|_1 = \|f\|_{-1}. \quad (2.6)$$

This implicitly defines the H^{-1} norm, although the definition then requires the solution of a Poisson problem. For example, in the previous example where $u_k = \sin(k\pi x)$ and the associated right hand side corresponding to the eigenfunction is $f_k = -\Delta u_k = (k\pi)^2 \sin(k\pi x) = (k\pi)^2 u_k$. We have already estimated that $|u_k|_1 = \frac{\pi k}{\sqrt{2}}$ and therefore $\|u_k\|_{-1} = \frac{1}{\sqrt{2}k\pi}$. We notice that the $\|\cdot\|_1$ norm weights high frequency oscillations heavily (linear in k), whereas the $\|\cdot\|_{-1}$ does not (it scales as $1/k$). On the other hand L^2 weights oscillations at all frequencies equally.

Let us now generalize these considerations and consider a matrix (or differential operator) A which is symmetric and positive. A has positive and real

eigenvalues and defines an inner product which may be represented in terms of eigenvalues and eigenfunctions. Let λ_i and u_i be the eigenvalues and eigenfunctions such that

$$Au_i = \lambda_i u_i$$

Then, x may be expanded in terms of the eigenfunctions u_i as $x = \sum_i c_i u_i$, where $c_i = (x, u_i)$, and we obtain

$$(x, x)_A = (Ax, x) = (A \sum_i c_i u_i, \sum_j c_j u_j) = (\sum_i \lambda_i c_i u_i, \sum_j c_j u_j)$$

Because A is symmetric, the eigenfunctions u_i are orthogonal to each other and we may choose a normalized basis such that $(u_i, u_j) = \delta_{ij}$. With this normalization, we simply obtain

$$\|x\|_A^2 = (x, x)_A = (Ax, x) = (A \sum_i c_i u_i, \sum_j c_j u_j) = \sum_i \lambda_i c_i^2$$

A generalization of the A -inner product (with corresponding norm) to a A^q -inner product that allow for both negative and fractional q is then as follows

$$\|x\|_{A,q}^2 = (x, x)_{A,q} = \sum_i \lambda_i^q c_i^2. \quad (2.7)$$

Clearly, this definition yields that $|u_k|_1 = \frac{\pi k}{\sqrt{2}}$ and $\|u_k\|_{-1} = \frac{1}{\sqrt{2k\pi}}$, as above.

As mentioned in Section 2.7, care has to be taken in finite element methods if the discrete eigenvalues are to correspond with the continuous eigenvalues. We will therefore detail the computation of negative and fractional norms in the following. Let λ_i and u_i be the eigenvalues and eigenvectors of the following generalized eigenvalue problem

$$Au_i = \lambda_i Mu_i \quad (2.8)$$

and let U be the matrix with the eigenvectors as columns. The eigenvalues are normalized in the sense that

$$U^T MU = I$$

where I is the identity matrix. We obtain

$$U^T AU = A \quad \text{or} \quad A = MUA(MU)^T,$$

where Λ is a matrix with the eigenvalues λ_i on the diagonal. Hence also in terms of the generalized eigenvalue problem (2.8) we obtain the A -norm as

$$\|x\|_A^2 = x^T MU \Lambda (MU)^T x$$

and we may define fractional and negative norms in the same manner as (2.7), namely that

$$\|x\|_{A,M,q}^2 = x^T MU \Lambda^q (MU)^T x.$$

Defining negative and fractional norms in terms of eigenvalues and eigenvectors is convenient for small scale problems, but eigenvalue problems are computationally demanding. It may, however, be tractable on subdomains, such as surfaces or interfaces of larger problems. There are however more efficient ways of computing such norms and operators, but those are beyond the scope of this book.

Computing the H^1 , L^2 , and H^{-1} norms

Let us consider $\Omega = (0, 1)$ and $u_k = \sin(\pi k x)$. Table 2.2 shows the H^1 , L^2 , and H^{-1} norms as computed with (2.7) with $q = 1, 0$, and -1 , respectively. Comparing the norms computed with the below code and shown in Table 2.1 with the norms calculated analytically on page 24, we see that the above definition (2.7) reproduces the H^1 and L^2 norms with $q = 1$ and $q = 0$, respectively. We also remark that while the H^1 norm increases as k increases, the H^{-1} norm demonstrates a corresponding decrease. Below we show the code for computing these norms.

$k \backslash \text{norm}$	$H^1, q = 1$	$L^2, q = 0$	$H^{-1}, q = -1$
1	2.2	0.71	0.22
10	22	0.71	0.022
100	222	0.71	0.0022

Table 2.2 The L^2 , L^7 , and H^1 norms of $\sin(k\pi x)$ for $k=1, 10$, and 100 .

```
from dolfin import *
from numpy import matrix, diagflat, sqrt
from scipy import linalg, random

def boundary(x, on_boundary): return on_boundary
```



```

mesh = UnitIntervalMesh(200)
V = FunctionSpace(mesh, "Lagrange", 1)
u = TrialFunction(V)
v = TestFunction(V)
bc = DirichletBC(V, Constant(0), boundary)

A, _ = assemble_system(inner(grad(u), grad(v))*dx, Constant(0)*v*dx, bc)
M, _ = assemble_system(u*v*dx, Constant(0)*v*dx, bc)
AA = matrix(A.array())
MM = matrix(M.array())

l, v = linalg.eigh(AA, MM)
v = matrix(v)
l = matrix(diagflat(l))

for k in [1, 10, 100]:
    u_ex = Expression("sin(k*pi*x[0])", k=k)
    u = interpolate(u_ex, V)
    x = matrix(u.vector().array())

    H1_norm = pi*k*sqrt(2)/2
    print "H1 norm of sin(%d pi x) %e (exact)" % (k, H1_norm)

    H1_norm = sqrt(assemble(inner(grad(u), grad(u))*dx))
    print "H1 norm of sin(%d pi x) %e (|grad(u)|^2)" % (k, H1_norm)

    H1_norm = sqrt(x*AA*x.T)
    print "H1 norm of sin(%d pi x) %e (x A x' )" % (k, H1_norm)

    W = MM.dot(v)
    H1_norm = sqrt(x*W*l*W.T*x.T)
    print "H1 norm of sin(%d pi x) %e (eig)" % (k, H1_norm)

    print ""

    L2_norm = sqrt(2)/2
    print "L2 norm of sin(%d pi x) %e (exact)" % (k, L2_norm)

    L2_norm = sqrt(assemble(u**2*dx))
    print "L2 norm of sin(%d pi x) %e |u|^2" % (k, L2_norm)

    L2_norm = sqrt(x*MM*x.T)
    print "L1 norm of sin(%d pi x) %e (x M x' )" % (k, L2_norm)

```

```

W = MM.dot(v)
L2_norm = sqrt(x*W*1**0*W.T*x.T)
print "L2 norm of sin(%d pi x) %e (eig)          " % (k,
                                                    L2_norm)

print ""

Hm1_norm = sqrt(2)/2/k/pi
print "H^-1 norm of sin(%d pi x) %e (exact)      " % (k,
                                                    Hm1_norm)
Hm1_norm = sqrt(x*W*1**-1*W.T*x.T)
print "H^-1 norm of sin(%d pi x) %e (eig)        " % (k,
                                                    Hm1_norm)
Hm1_norm = sqrt(x*MM*linalg.inv(AA)*MM*x.T)
print "H^-1 norm of sin(%d pi x) %e (x inv(A) x') " % (k,
                                                    Hm1_norm)

```

Remark 2.2 **Norms for $|q| > 1$.**

The norm (2.7) is well defined for any $|q| > 1$, but will not correspond to the corresponding Sobolev spaces.

2.10 Boundary conditions, Traces and Fractional Sobolev Spaces

In order to make sense of for instance boundary conditions we need to restrict from a domain Ω to its lower dimensional boundary $\partial\Omega$. Hence, for instance if Ω is the unit square in 2D then $\partial\Omega$ consists of the 1D lines that connect the vertices at the boundary of the unit square. However, a 1D line is infinitely thin and has no measure in 2D. As such, in $L^p(\Omega)$ the values at $\partial\Omega$ can be anything and still have no measurable impact on the $L_p(\Omega)$ norm of the function since the measure is zero.

However, functions in the Sobolev spaces $W^{k,p}$ have extra smoothness in terms of the requirements on derivatives. Therefore, values at lower dimensional manifolds may sometimes be well-defined. In fact, we need to be able to assign values on lower dimensional manifolds to enforce Dirichlet conditions. In order to make sense of values at lower dimensional manifolds we need the mathematical constructs of traces and fractional Sobolev spaces. Specifically, let $T : \Omega \rightarrow \partial\Omega$ be the so-called trace operator and $u \in w^{k,p}(\Omega)$ then

from Sobolev space theory it is well known that $Tu \in W^{k-1/2,p}(\partial\Omega)$ [7]. Typically, when finite element methods are used for single-physics problems then there is no need to pay attention to the fractional norms when implementing the boundary conditions. Boundary conditions are assigned at the boundary in a straightforward way as will be discussed in the next chapter. However, for multi-physics problems, care may be required for efficient and accurate simulation.

2.11 Exercises

Exercise 2.1 What is a norm? Show that

$$\|u\|_p = \left(\int_{\Omega} |u|^p dx \right)^{1/p}.$$

defines a norm on $L^p(\Omega)$.

Exercise 2.2 What is an inner product? Show that

$$(u, v)_k = \sum_{i \leq k} \int_{\Omega} \left(\frac{\partial u}{\partial x} \right)^i \left(\frac{\partial v}{\partial x} \right)^i dx.$$

defines an inner product on $H_0^1(\Omega)$ for $\Omega = (0, 1)$.

Exercise 2.3 Compute the H^1 and L^2 norms of a random function with values in $(0, 1)$ on meshes representing the unit interval of width 10, 100, and 1000 cells.

Exercise 2.4 Compute the H^1 and L^2 norms of $\sin(k\pi x)$ on the unit interval analytically and compare with the values presented in Table ??.

Exercise 2.5 Compute the H^1 and L^2 norms of the hat function in Picture 2.2.

Exercise 2.6 Consider the following finite element function u defined as

$$u = \begin{cases} \frac{1}{h}x - \frac{1}{h}(0.5 - h), & x = (0.5 - h, 0.5) \\ -\frac{1}{h}x + \frac{1}{h}(0.5 + h), & x = (0.5, 0.5 + h) \\ 0, & \text{elsewhere} \end{cases}$$

That is, it corresponds to the hat function in Figure 2.2, where $u(0.5) = 1$ and the hat function is zero every where in $(0, 0.5 - h)$ and $(0.5 + h, 1)$. Compute the H^1 and L^2 norms of this function analytically, and the L^2 , H^1 and H^{-1} norms numerically for $h = 10, 100$ and 1000 .

Chapter 3

Some common finite elements

3.1 Introduction

There is a jungle of finite elements that have been invented since the early 1940s, and we will not here give a comprehensive description of the topic. Instead, we will try to motivate the method by rather simple examples before we discuss some of the general features. The formal definition of a finite element, according to Ciarlet [4] is:

Definition A finite element is defined by a triplet (T, V, D) , where

- T is a bounded domain in \mathbb{R}^d , most typically a polyhedron;
- $V = \{\psi_i\}_{i=1}^n$ is a set of linearly independent basis functions on T ;
- $D = \{d_i\}_{i=1}^n$ is a set of (linearly independent) degrees of freedom defined in terms of linear functionals on V . (We remark for $v \in V$ we may evaluate $d_i(v)$ since d_i is a linear functional on V .) \square

As we see, the term "finite element" refers not only to the cells of the mesh, but also the function space and associated degrees of freedom. The definition is quite abstract, but as we will see, the definition encapsulates precisely what is needed in order to define a numerical method on a mesh.

Further, most finite elements are implemented in terms of its *nodal basis*. The nodal basis is defined as follows:

Definition The nodal basis for the triplet (T, V, D) is defined as the set of basis functions $\{\phi_i\}_{i=1}^n$ that satisfies

$$d_j(\phi_i) = \delta_{ij}, \quad \text{for } 1 \leq i, j \leq n.$$

The $\{d_j\}_{j=1}^n$ is often called the dual basis of the finite element. \square

3.2 Some example finite elements: Lagrange and Hermite on the unit interval.

Let us now try to make this concrete in a couple of simple examples. First we notice that in the above, we have two function spaces $\{\psi_i\}$ and $\{\phi_i\}$. Clearly,

$$\phi_i = \sum \alpha_{ij} \psi_j,$$

where the matrix α_{ij} is determined such that

$$d_i(\phi_j) = d_i\left(\sum \alpha_{ij} \psi_j\right) = \delta_{ij}.$$

Hence, let then $V = \mathbb{P}_k$, the space of polynomials of order up to k , and let's consider the Lagrange and Hermite elements, defined in terms of Lagrange and Hermite interpolation, respectively. On the unit interval

$$\mathbb{P}_k = \{1, x, \dots, x^k\}.$$

Clearly, \mathbb{P}_k has $k+1$ basis functions and they are all linearly independent. The Lagrange and Hermite elements are then defined in the examples below.

Example (The Lagrange element in 1D.) Lagrange interpolation is defined simply by nodal values in a set of points. Hence, let

$$x_j = j\Delta x, \quad \Delta x = \frac{1}{k}, \quad j = 0, \dots, k$$

Then the j 'th Lagrange function $L_j(x)$ can be written as a linear combination of the basis of \mathbb{P}_k as

$$L_j(x) = \sum_{i=0}^k \alpha_{ij} x^i$$

where α_{ij} are determined by

$$d_i(L_j) = L_j(x_i) = \sum_{i=0}^k \alpha_{ij} x_i^i = \delta_{ij}.$$

From this linear system we may calculate the α_{ij} for each specific basis function.

In 1D, an explicit formulation can be derived for L_j , namely

$$L_j(x) = \frac{x - x_0}{x_j - x_0} \dots \frac{x - x_{j-1}}{x_j - x_{j-1}} \dots \frac{x - x_{j+1}}{x_j - x_{j+1}} \dots \frac{x - x_k}{x_j - x_k}$$

Clearly, for instance $L_j(x_0) = 0$ whereas $L_j(x_j) = 1$. □

The Lagrange element can be written up in terms of an explicit formula in 1D, but is harder in higher dimensions. Therefore, we provide a simple code here that illustrates how such elements may be implemented. The below code is conceptually similar to the finite element tabulators used in FEniCS [9, 8, 1]. The following code computes the basis directly from the abstract definition without references to the above formula, using SymPy.

```
from sympy import *

def dirac(i,j):
    if i == j: return 1
    else: return 0

k = 5
x = Symbol("x")
dx = 1/k

basis = [x**j for j in range(0, k+1)]
points = [j*dx for j in range(0, k+1)]
dofs = symbols("a:%d"%(k+1))

print ("A polynomial space          ", basis)
print ("Points for the nodal basis ", points)
print ("The degrees of freedom (symbols) ", dofs)

pol = sum([dofs[i]*basis[i] for i in range(0, (k+1))])
print ("A generic polynomial          ", pol)

Lagrange_basis = []
for i in range(0, (k+1)):
    equations = []
    for j in range(len(points)):
        p = points[j]
        eq = pol.subs(x,p) - dirac(i,j)
        equations.append(eq)
    coeff = solve(equations, dofs)
    Nj = pol.subs(coeff)
```

```

Lagrange_basis.append(Nj)

for i, basis in enumerate(Lagrange_basis):
    print ("basis ", i, " ", Lagrange_basis[i])

# check that the Lagrange basis is what it is supposed to be
for i, basis in enumerate(Lagrange_basis):
    for j, point in enumerate(points):
        print ("i,j ", i,j, " basis evaluation ", "%0.3f" %
                basis.subs({ x: point}))

```

The output is as follows:

```

A polynomial space      [1, x, x**2, x**3, x**4, x**5]
Points for the nodal basis [0.0, 0.2, 0.4, 0.6000000000000001,
                           0.8, 1.0]
The degrees of freedom (symbols) (a0, a1, a2, a3, a4, a5)
A generic polynomial      a0 + a1*x + a2*x**2 + a3*x**3 + a4
                           *x**4 + a5*x**5
basis  0      -26.04166666666667*x**5 + 78.125*x**4 ....
basis  1      130.20833333333333*x**5 - 364.5833333333333*x**4 ....
...
i,j    0 0      basis evaluation    1.000
i,j    0 1      basis evaluation    0.000
...

```

The 6 basis functions of the Lagrange element of order 5 is shown in Fig. 3.1. Exercise 3.2 will consider a code for defining a Lagrange element of arbitrary order on a reference triangle.

The Hermite interpolation generalize the Lagrange interpolation by including also the first order derivative. As such the Hermite element is defined in terms of the Hermite interpolation. This is detailed in the following example:

Example The Hermite element in 1D. Let us consider the Hermite interpolation onto $k + 1$ points. Each point is associated with two degrees of freedom, the function evaluation and the evaluation of the first derivative of the function. using m derivatives in each point. Hence, the number of degrees of freedom, or the number of equations defined by the specification of the nodal basis in Definition 3.1.2 are then $2(k + 1)$. As such our polynomial space would be $\mathbb{P}_{2(k+1)}$. We may compute the nodal basis of the Hermite element: Let H_j be the j 'th nodal basis, expressed as

$$H_j = \sum_i \alpha_{ij} x^i$$

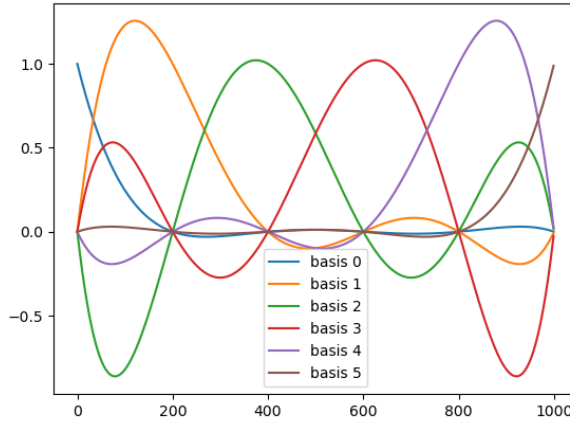


Fig. 3.1 The basis function of the Lagrange element of order 5.

Then where α_{ij} are determined by

$$d_i(L_j) = L_j(x_i) = \delta_{ij}.$$

Here, let's split the degrees of freedom into even and odd numbers, where the even numbering refers to point evaluations whereas the odd numbers are the evaluation of the derivatives. That is

$$\begin{aligned} d_i(H_j) &= H_j(x_i) &= \delta_{ij}, & \text{even } i, j \\ d_i(H_j) &= H'_j(x)|_{x=x_i} &= \delta_{ij}, & \text{odd } i, j \end{aligned}$$

3.3 Mapping a reference element onto a physical element.

There are a couple of observations that makes the above definition of the finite element really useful. First, let's consider the mappings from a reference element to a physical element. A crucial observation is the fact that the mapping between an arbitrary cell of a general mesh and the reference cell can be

generalized to a mapping between an arbitrary finite element on the mesh and a corresponding reference element. This observation is detailed below.

Let x and \hat{x} be coordinates in the domains T and \hat{T} , respectively, and for simplicity we assume an affine mapping between the coordinates:

$$x = F_T(\hat{x}) = A_T \hat{x} + x_0$$

The Jacobian of the mapping is

$$\frac{\partial x}{\partial \hat{x}} = J(\hat{x}) = A_T$$

For isoparametric elements, a basis function ϕ is the simply defined in terms of its associated function $\hat{\phi}$ on the reference element, ie.

$$\phi(x) = \hat{\phi}(\hat{x}).$$

With this definition we may easily evaluate integrals involving the basis functions:

$$\int_T \phi(x) dx = \int_{\hat{T}} \hat{\phi}(\hat{x}) \det J d\hat{x},$$

where $\det J$ is the determinant of J . Furthermore, derivatives of the basis functions are readily available by using the chain-rule:

$$\frac{\partial \phi}{\partial x_i} = \sum_j \frac{\partial \hat{\phi}}{\partial \hat{x}_j} \frac{\partial \hat{x}_j}{\partial x_i}$$

As such the finite element engines may perform all the computations on the reference cells, which makes the implementation easy and efficient.

3.4 The connectivity of the mesh and the corresponding finite element space

The Lagrange element of order 5 was illustrated in Fig. 3.1. We observe here that the basis function 0 and 5 are associated with the edges $x = 0$ and $x = 1$, respectively. The other functions are all zero at the edges. Hence, the basis function 1, ..., 4 do not connect to any other element, whereas the basis 0 would directly connect to the a corresponding element on the left whereas basis

5 connects to the an element on the right, if present. Hence the edge nodes defines the connectivity and hereby the continuity towards the neighbouring elements.

The situation is more complicated in 2D and 3D. Consider the Lagrange element of 1, 2, and 3 order in Fig. 3.4. Black, blue and red circles mark the vertex, edge and interal nodes, which through the connectivity of the mesh defines the connectivity of the finite element filed. Consider the mesh in Fig. 3.4. Clearly, the vertex node in the center, marked by a black circle is connected to all the 8 neighbouring elements. Hence, the corresponding basis function ties these eight elements together.

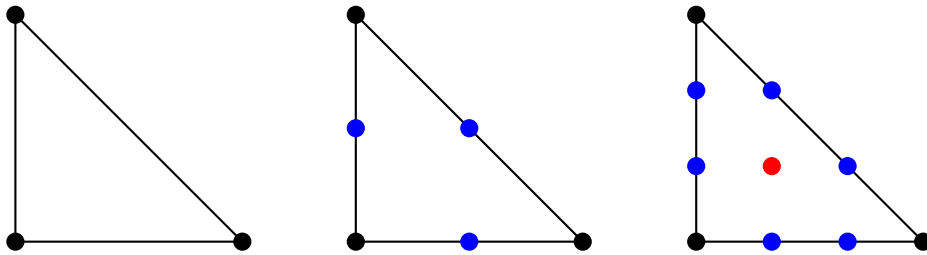


Fig. 3.2 The Lagrange element of order 1, 2, 3 on the reference triangle in 2D. Black circles mark the vertex nodes, blue the edge nodes and red the internal nodes.

KAM: Describe how to make Vector elements from scalar elements

KAM: Describe also briefly CR, RT, Nedgelec, MTW elements

3.5 Exercises

Exercise 3.1 Make a Python code that defines a Hermite on the unit interval.

Exercise 3.2 Make a Python code that defines a Lagrange element of arbitrary order on the reference triangle consisting of the vertices $(0, 0)$, $(1, 0)$ and $(0, 1)$. Let $\mathbb{P}_k = \{x^i y^j\}$ for i, j such that $i + j \leq k$

Exercise 3.3 Check that the interpolation result of the Bramble-Hilbert lemma 2.4 applies to the Lagrange interpolation on the unit line. Consider for example a function $f = \sin(x)$ on the unit interval. The function f is a

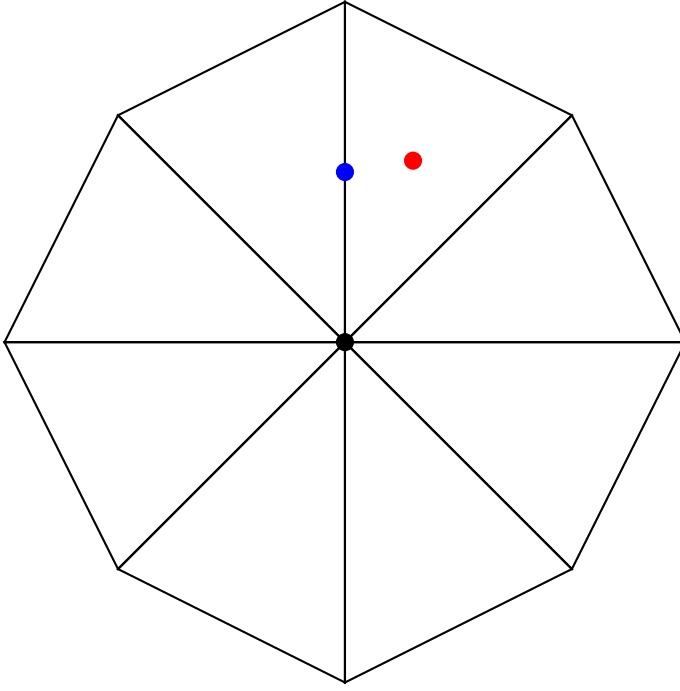


Fig. 3.3 A simple mesh with 8 triangles all meeting at a common point. Here, we have marked (only) three nodes associated with a third order Lagrange element: A vertex node (black), an edge node (blue) and an internal node (red). Marking all nodes would yield 9 vertex nodes, 16 edge nodes, and 8 internal nodes.

good example as it cannot be expressed as a polynomial of finite order, but can be approximated arbitrary well.

Exercise 3.4 Compute the condition number of the mass matrix when using the Lagrange and the Hermite basis. Compare it with the condition number when using the basis consisting of monomials, ie. $(1, x, x^2, \dots)$. The mass matrix on the unit interval is the matrix $M_{ij} = \int_0^1 \phi_i \phi_j dx$ where $\{\phi_i\}$ is the set of basis functions in use.

Chapter 4

The finite element method for elliptic problems

4.1 The weak formulation and the finite element formulation

We are now in position to analyze the finite element method for an elliptic problem in detail and provide rigorous estimates on the numerical accuracy. We remember the strong formulation: Find the solution u of the problem

$$-\nabla \cdot (k \nabla u) = f \quad \text{in } \Omega, \quad (4.1)$$

$$u = g \quad \text{on } \partial\Omega_D, \quad (4.2)$$

$$k \frac{\partial u}{\partial n} = h \quad \text{on } \partial\Omega_N, \quad (4.3)$$

where we assume $\partial\Omega = \partial\Omega_D \cup \partial\Omega_N$ and $\partial\Omega_D \cap \partial\Omega_N = \emptyset$.

In order to arrive at the weak formulation, we introduce two Sobolev spaces

$$H_{0,D}^1(\Omega) = \{u \in H^1(\Omega) \mid Tu = 0 \text{ on } \partial\Omega_D\}, \quad (4.4)$$

$$H_{g,D}^1(\Omega) = \{u \in H^1(\Omega) \mid Tu = g \text{ on } \partial\Omega_D\}. \quad (4.5)$$

Here, both spaces are subspaces of the H^1 space introduced in the previous chapter. The subspaces include only the functions with appropriate values on the Dirichlet part of the boundary $\partial\Omega_D$. As detailed in Chapter 1.1, we obtain the weak formulation by 1) multiplying the equation (4.1) with a test function v , 2) employing Gauss-Green's lemma, and 3) employing the boundary conditions.

We arrive at the following *weak formulation*, which includes the precise definitions of spaces of the trial and test functions, source function and boundary conditions:

Given $f \in H_D^{-1}(\Omega)$, $h \in H^{-1/2}(\partial\Omega_N)$, find $u \in H_{g,D}^1(\Omega)$ such that

$$\int_{\Omega} (k \nabla u) \cdot \nabla v \, dx = \int_{\Omega} f v \, dx + \int_{\partial\Omega_N} h v \, ds, \quad \forall v \in H_{0,D}^1(\Omega). \quad (4.6)$$

Here, the negative norms are similar to the negative norms introduced in the previous chapter, although we there had Dirichlet conditions on the complete boundary. Alternatively, and perhaps simpler from a mathematical point of view is to define it in terms of duality as in Remark 2.8.1. When implementing the method, we seldom need to pay attention to what space our source and boundary condition functions reside in, but we remark that it is sometimes useful to include functions that are not defined in points but only through integration over elements.

In order to define a finite element method, let Ω_h be a mesh covering Ω , consisting of a set E_h of cells. For simplicity, we assume that the cells are simplices (triangles in 2D, tetrahedrons in 3D). Simplices fit very well with standard polynomials, so let \mathcal{P}_k be the space of polynomials of order k , i.e., a basis in 2D could be $\{x^i y^j\}_{i,j|i+j \leq k}$. A corresponding finite element method consist of some trial and test spaces

$$V_{h,0} = \{u \in H_{0,D}^1(\Omega) \mid \forall e \in E_h, u|_e \in \mathcal{P}_k\}, \quad (4.7)$$

$$V_{h,g} = \{u \in H_{g,D}^1(\Omega) \mid \forall e \in E_h, u|_e \in \mathcal{P}_k\}. \quad (4.8)$$

KAM: perhaps instead introduce Lagrange elements

The corresponding finite element formulation is then:

Given $f \in H_D^{-1}$, $h \in H^{-1/2}(\partial\Omega_N)$, find $u_h \in V_{h,g}$ such that

$$\int_{\Omega} (k \nabla u_h) \cdot \nabla v_h \, dx = \int_{\Omega} f v_h \, dx + \int_{\partial\Omega_N} h v_h \, ds, \quad \forall v \in V_{h,0}. \quad (4.9)$$

4.2 What is an elliptic equation ?

An elliptic partial differential equation is *strictly positive* with respect to some inner product. In order to show that (4.6) is elliptic, we will need three concepts: Poincaré's inequality, lifting, the positivity of k .

Lifting, which is often used for theoretical purposes but seldom in implementation, refers to changing the problem from having non-homogenous Dirichlet conditions to homogenous Dirichlet conditions. Let us assume that G is a function in $H^1(\Omega)$ such that $Tu|_{\partial\Omega_D} = g$. Clearly, there are infinitely many such functions and in many cases it is easy to find such a G . Then, by linearity, $u = u_0 + G$ solves (4.1)–(4.3) with u_0 defined as

$$-\nabla \cdot (k \nabla u_0) = f + \nabla \cdot (k \nabla G) \quad \text{in } \Omega, \quad (4.10)$$

$$u_0 = 0 \quad \text{on } \partial\Omega_D, \quad (4.11)$$

$$k \frac{\partial u_0}{\partial n} = h - k \frac{\partial G}{\partial n} \quad \text{on } \partial\Omega_N. \quad (4.12)$$

Hence, the purpose of the lifting is clear: It transforms a problem with non-homogenous Dirichlet conditions, in which the Poincaré's lemma cannot be applied, to a problem with homogenous Dirichlet conditions where Poincaré's lemma can be applied. It is used for theoretical purposes, but since G can be chosen arbitrarily as long as it fits the boundary conditions, the procedure does not impose significant constraints on the analysis. Most analysis therefore only deals with the case of homogenous Dirichlet conditions (see e.g. [2] for more detailed coverage).

In order for (4.1) (or (4.10)) to be an elliptic problem, with $k(x) \in \mathbb{R}^{d \times d}$ given $\Omega \in \mathbb{R}^d$, k needs to be strictly positive and bounded for all $x \in \Omega$. That is:

For $\forall \xi \in \mathbb{R}^n$ and $\forall x \in \Omega$ there exists a $k_0 > 0$ and $k_1 < \infty$ such that

$$k_0 |\xi|^2 \leq \xi^T k(x) \xi \leq k_1 |\xi|^2.$$

Given that Poincaré's inequality applies and that k is strictly positive and bounded as defined above, then

$$\int_{\Omega} (k \nabla u) \cdot \nabla v \, dx$$

defines an inner product on $H_{0,D}^1(\Omega)$. The result is crucial in this book and is hence left as a series of Exercises 4.1–4.5. The exercises show that

$$\int_{\Omega} (k \nabla u) \cdot \nabla v \, dx, \quad (4.13)$$

$$\int_{\Omega} (\nabla u) \cdot \nabla v \, dx, \quad (4.14)$$

$$\int_{\Omega} uv + (k \nabla u) \cdot \nabla v \, dx, \quad (4.15)$$

$$\int_{\Omega} uv + (\nabla u) \cdot \nabla v \, dx. \quad (4.16)$$

are all equivalent inner products on $H_{0,D}^1(\Omega)$.

4.3 An *a priori* Error Estimate

In the previous chapter we listed some approximation properties of polynomials in general. We will now employ these results in order to derive *a priori* error estimates. To achieve this we will need that the equation is elliptic and in addition the concept of Galerkin orthogonality.

Inner products are extraordinary useful as they introduce a geometry of the space. For instance, a function may be orthogonal to another function. This leads us to our fourth concept: Galerkin orthogonality. The concept is simple, let the numerical error be $e_h = u - u_h$. Then we remark that $v_h \in V_{h,g} \subset H_{g,D}^1$. Hence, letting $v = v_h$ in (4.6) and subtracting (4.9) we obtain:

$$\int_{\Omega} (k \nabla (u - u_h)) \cdot \nabla v_h \, dx = \int_{\Omega} (f - f) v_h \, dx + \int_{\partial \Omega_N} (h - h) v_h \, ds = 0 \quad \forall v \in V_{h,0}. \quad (4.17)$$

That is, the numerical error $e_h = u - u_h$ is orthogonal to all test functions v_h used by the finite element method. This is a strong result and perhaps surprising. The solution u_h , found by solving (4.9) is therefore the best possible solution that can be found in $V_{h,g}$.

Since, $\int_{\Omega} (k \nabla u) \cdot \nabla v \, dx$ defines an inner product and associated norm, equivalent with the standard H_0^1 norm we can employ the approximation result (2.4) Chapter 2. The results is called Cea's lemma, and we will later see it in a more general context. Here, we briefly prove an error estimate. First, we remark that, as found in the Exercises below

$$k_0 \int_{\Omega} (\nabla u)^2 \, dx \leq \int_{\Omega} (k \nabla u) \cdot \nabla u \, dx \leq k_1 \int_{\Omega} (\nabla u)^2 \, dx,$$

As such

$$\begin{aligned}
 k_0 \int_{\Omega} (\nabla(u - u_h))^2 dx &\leq \int_{\Omega} (k \nabla(u - u_h)) \cdot \nabla(u - u_h) dx \\
 &\leq \int_{\Omega} (k \nabla(u - u_h)) \cdot \nabla(u - P_m u + P_m u - u_h) dx, \\
 &\leq \int_{\Omega} (k \nabla(u - u_h)) \cdot \nabla(u - P_m u) dx \\
 &\leq k_1 \int_{\Omega} (\nabla(u - u_h)) \cdot \nabla(u - P_m u) dx
 \end{aligned}$$

Here, we use that we may subtract and add $P_m u$ which totals to zero, and remark that both u_h and $P_m u$ are in $V_{h,0}$ and hence both are orthogonal to $u - u_h$ as in (4.17). Further, by using Cauchy-Schwarz inequality, which in this case states that

$$\begin{aligned}
 &\int_{\Omega} (\nabla(u - u_h)) \cdot \nabla(u - P_m u) dx \\
 &\leq \left(\int_{\Omega} (\nabla(u - u_h))^2 dx \right)^{1/2} \left(\int_{\Omega} \nabla(u - P_m u)^2 dx \right)^{1/2}
 \end{aligned}$$

we immediately have by the Bramble-Hilbert lemma (2.4) that

$$\left(\int_{\Omega} (\nabla(u - u_h))^2 dx \right)^{1/2} \leq \frac{k_1}{k_0} \left(\int_{\Omega} \nabla(u - P_m u)^2 dx \right)^{1/2} \leq \frac{k_1}{k_0} Ch^{m-1} |u|_m \quad (4.18)$$

Estimating the convergence rate

Let us consider the Poisson problem, $-\Delta u = f$, on the unit interval with homogenous Dirichlet conditions with a manufactured solution $u = \sin(k\pi x)$ such that we can check the convergence rate. Let us consider the Lagrange element of various orders. From the above Cea's lemma we an error rate of m in the H^1 -seminorm. The following code implements a solver and estimates the rates.

```

from dolfin import *

def boundary (x): return x[0] < DOLFIN_EPS or x[0] > 1 -
                        DOLFIN_EPS

```

```

f = Expression("M_PI*M_PI*sin(M_PI*x[0])", degree=P+5)
u_analytical = Expression("sin(M_PI*x[0])", degree=P+5)

Ns = [4, 8, 16, 32, 64, 128, 256]
Ps = [1, 2, 3, 4]
L2_errors = {}

for P in Ps:
    for N in Ns:
        mesh = UnitIntervalMesh(N)
        h = mesh.hmax()
        V = FunctionSpace(mesh, "Lagrange", P)
        u = TrialFunction(V)
        v = TestFunction(V)

        # bc
        u0 = Constant(0)
        bc = DirichletBC(V, u0, boundary)

        a = inner(grad(u), grad(v))*dx
        L = f*v*dx

        U = Function(V)
        solve (a ==L, U, bc)

        L2_error = assemble(pow(U-u_analytical, 2)*dx)
        L2_error = sqrt(L2_error)

        L2_errors[(P, N)] = (h, L2_error)

# numbers to estimate the rates
for P in Ps:
    for i in range(len(Ns)-1):
        print ("P ", P, L2_errors[(P, Ns[i])][1] / L2_errors[(
            P, Ns[i+1])][1])

# log-log plot for assessing whether the convergence rate is
# polynomial and what the rate is
from numpy import log
import matplotlib.pyplot as plt
for P in Ps:
    hs = []
    errors = []
    for N in Ns:
        h, error = L2_errors[(P, N)]
        hs.append(h)

```

```

        errors.append(error)
    plt.loglog(Ns, errors)
plt.show()

```

In Fig. 4.1 we show a log-log plot of the error for different mesh resolutions and element orders. The linear relationship shows that the error behaves in a polynomial fashion, except for the case with very small errors where we see stagnation due to round of errors. We remark that we assess the error in L^2 which rather than the H^1 . By inspection, we notice that the error rate is $m+1$, i.e. second order for linear elements.

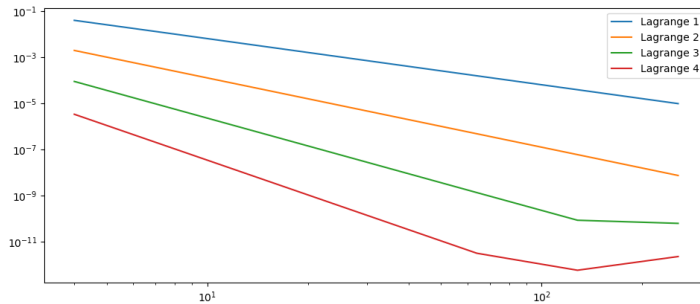


Fig. 4.1 The error for Lagrange elements of various orders in a log-log plot. The log-log plot shows a clear linear relationship for the various orders demonstrating polynomial order.

4.4 Exercises

Exercise 4.1 Let $\Omega = (0, 1)$. Show that

$$a(u, v) = \int_{\Omega} u v \, dx$$

is a bilinear form.

Exercise 4.2 Let $\Omega = (0, 1)$. Show that

$$a(u, v) = \int_{\Omega} u v \, dx$$

forms an inner product.

Exercise 4.3 Let $\Omega = (0, 1)$ then for all functions in $H_0^1(\Omega)$ then Poincaré's inequality states that

$$|u|_{L^2} \leq C \left| \frac{\partial u}{\partial x} \right|_{L^2}$$

Use this inequality to show that the H^1 semi-norm defines a norm equivalent with the standard H^1 norm on $H_0^1(\Omega)$.

Exercise 4.4 Let $\Omega = (0, 1)$. Show that

$$a(u, v) = \int_{\Omega} \nabla u \cdot \nabla v \, dx$$

forms an inner product on $H_0^1(\Omega)$ equivalent with the standard $H^1(\Omega)$ inner product.

Exercise 4.5 Let $\Omega = (0, 1)$. Show that

$$a(u, v) = \int_{\Omega} k \nabla u \cdot \nabla v \, dx$$

forms an inner product on $H_0^1(\Omega)$ given that $k \in \mathbb{R}^{n \times n}$ is strictly positive and bounded. The inner product is equivalent with the $H_0^1(\Omega)$ inner product.

Chapter 5

Discretization of a convection-diffusion problem

5.1 Introduction

This chapter concerns convection-diffusion equations of the form:

$$\begin{aligned} -\mu\Delta u + w \cdot \nabla u &= f & \text{in } \Omega \\ u &= g & \text{on } \partial\Omega \end{aligned}$$

Here w is the velocity, μ is the diffusivity, and u is the unknown variable of interest. We assume the Dirichlet condition $u = g$ on the boundary, while f is a source term.

The problem is a singular perturbation problem for $|w| \gg \mu$. That is, the problem is well-posed for $\mu > 0$ but becomes over-determined by boundary conditions as μ tends to zero. In particular, for $\mu = 0$ the Dirichlet conditions should only be set on the inflow domain Γ ; that is, where $n \cdot w < 0$ for the outward unit normal n .

For many practical situations $\mu > 0$, but small in the sense that $\mu \ll |w|$. For such problems, the solution will often be similar to the solution of the reduced problem with $\mu = 0$ except close to the non-inflow boundary $\partial\Omega \setminus \Gamma$. Here, there will typically be a boundary layer $\exp(-\|w\|_\infty x / \mu)$. Furthermore, discretizations often show unphysical oscillations starting at this boundary layer.

The next example shows a 1D convection diffusion problem resulting in non-physical oscillations due to the use of a standard Galerkin approximation.

Standard Galerkin approximation

Consider the following 1D problem convection diffusion problem, where $w = -1$ for simplicity:

$$-u_x - \mu u_{xx} = 0, \quad (5.1)$$

$$u(0) = 0, u(1) = 1. \quad (5.2)$$

The analytical solution is:

$$u(x) = \frac{e^{-x/\mu} - 1}{e^{-1/\mu} - 1}.$$

Hence, for $\mu \rightarrow 0$, both $e^{-x/\mu}$ and $e^{-1/\mu}$ will be small and $u(x) \approx 1$ unless $x \approx 0$. However, close to the outflow boundary at $x = 0$, there will be a boundary layer where u has exponential growth.

We solve the problem with a standard Galerkin method using linear first order Lagrange elements. To be specific, the variational problem is:

Find $u \in H^1_{(0,1)}$ such that

$$\int_0^1 -u_x v + \mu u_x v_x dx = 0, \quad \forall v \in H^1_{(0,0)}.$$

Here, $H^1_{(0,1)}$ contains functions $u \in H^1$ with $u = 0$ at $x = 0$ and $u = 1$ and $x = 1$, while $H^1_{(0,0)}$ contains functions that are zero both at $x = 0$ and $x = 1$. We consider a $\mu = 0.01$, a relatively large μ , to enable us to see the differences on a relatively coarse mesh.

Both the numerical and analytical solutions are shown in Figure 5.1. Clearly, the numerical solution is polluted by non-physical oscillations on the coarse mesh with 10 elements, while a good approximation is obtained for 100 elements.

Finally, we show the complete code for this example:

```
from dolfin import *
for N in [10, 100]:

    mesh = UnitInterval(N)
    V = FunctionSpace(mesh, "CG", 1)

    u = TrialFunction(V)
    v = TestFunction(V)

    mu_value = 1.0e-2
    mu = Constant(mu_value)
```

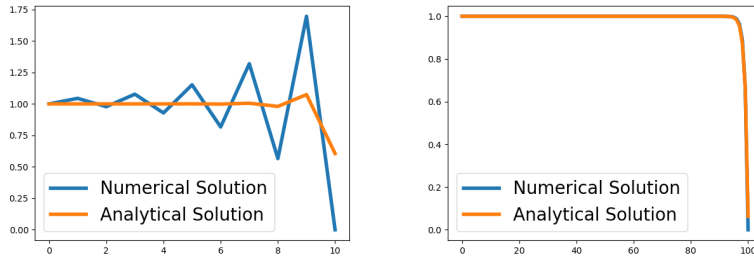


Fig. 5.1 Solution of the convection diffusion problem obtained with 10 and 100 elements. The left figure obtained on a mesh with 10 elements shows wild oscillations, while the mesh with 100 elements demonstrate a nicely converged solution.

KAM: wrong label to the left. Should be solution at N=10, 100

```
f = Constant(0)
h = mesh.hmin()

a = (-u.dx(0)*v + mu*u.dx(0)*v.dx(0))*dx
L = f*v*dx

u_analytical = Expression("(exp(-x[0]/%e) - 1)/ (exp(-1/%e) - 1)" % (mu_value, mu_value))

def boundary(x):
    return x[0] < DOLFIN_EPS or x[0] > 1.0 - DOLFIN_EPS

bc = DirichletBC(V, u_analytical, boundary)

U = Function(V)
solve(a == L, U, bc)

U_analytical = project(u_analytical, V)

import pylab
pylab.plot(U.vector().array())
pylab.plot(U_analytical.vector().array())
pylab.legend(["Numerical Solution", "Analytical Solution"])
pylab.show()
```

□

KAM: Coordinates in plotting is probably swapped.

To understand Example 5.1 we first remark that the discretization corresponds to the following central finite difference scheme:

$$-\frac{\mu}{h^2} [u_{i+1} - 2u_i + u_{i-1}] - \frac{w}{2h} [u_{i+1} - u_{i-1}] = 0, \quad i = 1, \dots, N-1$$

$$u_0 = 0, \quad u_N = 1$$

Above, we kept w as a variable such that we may discuss the directionality of upwinding in terms of the convection. Clearly, if $\mu = 0$ then the scheme reduces to

$$-\frac{w}{2h} [u_{i+1} - u_{i-1}] = 0, \quad i = 1, \dots, N-1$$

$$u_0 = 0, \quad u_N = 1$$

Here, it is clear that u_{i+1} is coupled to u_{i-1} , but not to u_i . Hence, this scheme allow for an alternating sequence of $u_{i+1} = u_{i-1} = \dots$, while $u_i = u_{i-2} = \dots$ resulting in oscillations.

One cure for these oscillations is upwinding. That is, instead of using a central difference scheme, we employ the following difference scheme:

$$\frac{du}{dx}(x_i) = \frac{1}{h} [u_{i+1} - u_i] \quad \text{if } w < 0,$$

$$\frac{du}{dx}(x_i) = \frac{1}{h} [u_i - u_{i-1}] \quad \text{if } w > 0.$$

Using this scheme, oscillations will disappear. The approximation will however only be first order.

There is a relationship between upwinding and artificial diffusion. If we discretize u_x with a central difference and add diffusion as $\epsilon = h/2\Delta$ we get

$$\begin{aligned} & \frac{u_{i+1} - u_{i-1}}{2h} \quad \text{central scheme, first order derivative} \\ & + \frac{h}{2} \frac{-u_{i+1} + 2u_i - u_{i-1}}{h^2} \quad \text{central scheme, second order derivate} \\ & = \frac{u_i - u_{i-1}}{h} \quad \text{upwind scheme} \end{aligned}$$

Hence, upwinding is equivalent to adding artificial diffusion with $\epsilon = h/2$; that is, in both cases we actually solve the problem

$$-(\mu + \epsilon)u_{xx} + w u_x = f.$$

using a central difference scheme.

Finite difference upwinding is difficult to express using finite elements methods, but it is closely to adding some kind of diffusion to the scheme. The next example shows the solution of the problem in Example 5.1 with artificial diffusion added.

Stabilization using artificial diffusion

Consider again the following 1D problem convection diffusion problem:

$$-u_x - \mu u_{xx} = 0, \quad (5.3)$$

$$u(0) = 0, u(1) = 1. \quad (5.4)$$

We solve the problem with a standard Galerkin method using linear first order Lagrange elements as before, but we add artificial diffusion. To be specific, the variational problem is:

Find $u \in H_{(0,1)}^1$ such that

$$\int_0^1 -u_x v + (\mu + \beta h)u_x v_x = 0, \quad \forall v \in H_{(0,0)}^1,$$

where $\beta = 0.5$ corresponds to the finite difference scheme with artificial diffusion mentioned above. Below is the code for the changed variational form:

```
beta_value = 0.5
beta = Constant(beta_value)
f = Constant(0)
h = mesh.hmin()
a = (-u.dx(0)*v + mu*u.dx(0)*v.dx(0) + beta*h*u.dx(0)*v.dx(0)) * dx
```

Figure 5.2 shows the solution for 10 and 100 elements when using artificial diffusion stabilization. Clearly, the solution for the coarse grid has improved dramatically since the oscillations have vanished and the solution appear smooth. It is, however, interesting to note that the solution for the fine mesh is actually less accurate than the solution in Fig 5.2 for the corresponding fine mesh. The reason is that the scheme is now first order, while the scheme in Example 5.1 is second order.

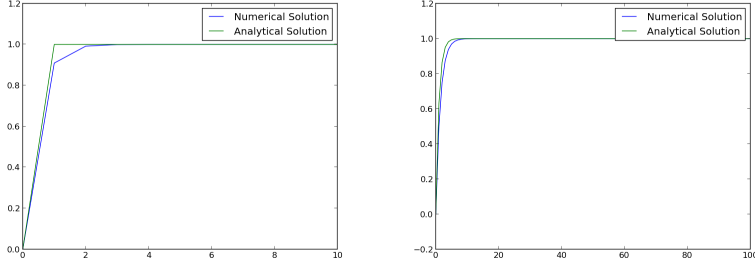


Fig. 5.2 Solution of the convection diffusion problem obtained with 10 and 100 elements using artificial diffusion to stabilize.

5.2 Streamline diffusion/Petrov-Galerkin methods

In the previous section we saw that artificial diffusion may be added to convection diffusion dominated problems to avoid oscillations. The diffusion was, however, added in a rather ad-hoc manner. Here, we will see how diffusion may be added in a consistent way; that is, without changing the solution as $h \rightarrow 0$. This leads us to streamline diffusion using the Petrov-Galerkin method. Our problem reads:

Find u such that

$$\begin{aligned} -\mu \Delta u + w \cdot \nabla u &= f \quad \text{in } \Omega, \\ u &= g \quad \text{on } \partial\Omega. \end{aligned}$$

The **weak formulation** reads:

Find $u \in H_g^1$ such that

$$a(u, v) = b(v) \quad \forall v \in H_0^1,$$

where

$$\begin{aligned} a(u, v) &= \int_{\Omega} \mu \nabla u \cdot \nabla v \, dx + \int_{\Omega} (w \cdot \nabla u) v \, dx, \\ b(v) &= \int_{\Omega} f v \, dx. \end{aligned}$$

Here, H_g^1 is the subspace of H^1 where the trace equals g on the boundary $\partial\Omega$.

The *standard Galerkin* discretization is:

Find $u_h \in V_{h,g}$ such that

$$a(u_h, v_h) = (f, v_h) \quad \forall v_h \in V_{h,0}. \quad (5.5)$$

Here, $V_{h,g}$ and $V_{h,0}$ are the subspaces with traces that equals g and 0 on the boundary, respectively.

Adding artificial diffusion to the standard Galerkin discretization, as was done in Example 5.1, can be done as:

Find $u_h \in V_{h,g}$ such that

$$a(u_h, v_h) + \frac{h}{2}(\nabla u_h, \nabla v_h) = (f, v_h) \quad \forall v_h \in V_{h,0}.$$

Let

$$\tau(u, v_h) = a(u_h, v_h) - (f, v_h).$$

Then the *truncation error* is first order in h ; that is,

$$\tau(u) = \sup_{v \in V_h, v \neq 0} \frac{\tau(u, v_h)}{\|v\|_V} \sim \mathcal{O}(h).$$

Hence, the scheme is *consistent* in the sense that

$$\lim_{h \rightarrow 0} \tau(u) \rightarrow 0.$$

However, it is not *strongly consistent* in the sense that $\tau(u) = 0$ for every discretization, which is what is obtained with the Galerkin method due to Galerkin-orthogonality:

$$\tau(u, v_h) = a(u_h, v_h) - (f, v_h) = a(u_h - h, v_h) = 0 \quad \forall v_h \in V_h.$$

The *Streamline diffusion/Petrov-Galerkin* method introduces a strongly consistent diffusion by employing alternative test functions. Let us therefore assume that we have a space of test functions W_h . Abstractly, the Petrov-Galerkin method appears very similar to the Galerkin method, that is:

Find $u_h \in V_{h,g}$ such that

$$a(u_h, v_h) = (f, v_h) \quad \forall v_h \in W_{h,0}.$$

Again, $V_{h,g}$ and $W_{h,0}$ are the subspaces with traces that equals g and 0 on the boundary, respectively. Notice that the only difference from the standard Galerkin formulation is that test and trial functions differ.

On matrix form, the standard Galerkin formulation reads:

$$A_{ij} = a(N_i, N_j) = \int_{\Omega} \mu \nabla N_i \cdot \nabla N_j \, dx + \int_{\Omega} (w \cdot \nabla N_i) N_j \, dx, \quad (5.6)$$

while for the Petrov Galerkin method, we use the test functions L_j :

$$A_{ij} = a(N_i, L_j) = \int_{\Omega} \mu \nabla N_i \cdot \nabla L_j \, dx + \int_{\Omega} (w \cdot \nabla N_i) L_j \, dx$$

A clever choice of L_j will enable us to add diffusion in a consistent way. To make sure that the matrix is still quadratic, we should however make sure that the dimension of V_h and W_h are equal.

Let L_j be defined as $L_j = N_j + \beta h (w \cdot \nabla N_j)$. Writing out the matrix A_{ij} in (5.6) now gives

$$\begin{aligned} A_{ij} &= a(N_i, N_j + \beta h (w \cdot \nabla N_j)) \\ &= \int_{\Omega} \mu \nabla N_i \cdot \nabla (N_j + \beta h w \cdot \nabla N_j) \, dx + \int_{\Omega} w \cdot \nabla N_i \cdot (N_j + \beta h w \cdot \nabla N_j) \, dx \\ &= \underbrace{\int_{\Omega} \mu \nabla N_i \cdot \nabla N_j \, dx + \int_{\Omega} w \cdot \nabla N_i N_j \, dx}_{\text{standard Galerkin}} \\ &\quad + \underbrace{\beta h \int_{\Omega} \mu \nabla N_i \cdot \nabla (w \cdot \nabla N_j) \, dx}_{=0 \text{ third order term, for linear elements}} + \underbrace{\beta h \int_{\Omega} (w \cdot \nabla N_i) (w \cdot \nabla N_j) \, dx}_{\text{Artificial diffusion in } w \text{ direction}} \end{aligned}$$

Notice that also the righthand side changes

$$b(L_j) = \int_{\Omega} f L_j \, dx = \int_{\Omega} f (N_j + \beta h w \cdot \nabla N_j) \, dx$$

Thus, both the matrix and the righthand side are changed such that artificial diffusion is added in a consistent way.

We summarize this derivation by stating the SUPG problem. Find $u_{h,sd} \in H_g^1$ such that

$$a_{sd}(u, v) = b_{sd}(v) \quad \forall v \in H_0^1, \quad (5.7)$$

where

$$\begin{aligned}
a_{sd}(u, v) &= \int_{\Omega} \mu \nabla u \cdot \nabla v \, dx + \int_{\Omega} (w \cdot \nabla u) v \, dx \\
&\quad + \beta h \int_{\Omega} (w \cdot \nabla u)(w \cdot \nabla v) \, dx + \beta h \mu \sum_e \int_{\Omega_e} -\Delta u (w \cdot \nabla v) \, dx, \\
b_{sd}(v) &= \int_{\Omega} f v \, dx + \beta h \int_{\Omega} f (w \cdot \nabla v) \, dx.
\end{aligned}$$

5.3 Well posedness of the continuous problem

Before we discuss error estimates of the discrete problem, we briefly describe the properties of the continuous problem.

Theorem 5.1 *Lax-Milgram theorem*

Let V be a Hilbert space, $a(\cdot, \cdot)$ be a bilinear form, $L(\cdot)$ a linear form, and let the following three conditions be satisfied:

1. $a(u, u) \geq \alpha \|u\|_V^2, \quad \forall u \in V,$
2. $a(u, v) \leq C \|u\|_V \|v\|_V, \quad \forall u, v \in V,$
3. $L(v) \leq D \|v\|_V, \quad \forall v \in V.$

Then the problem: Find $u \in V$ such that

$$a(u, v) = L(v) \quad \forall v \in V.$$

is well-posed in the sense that there exists a unique solution with the following stability condition

$$\|u\|_V \leq \frac{C}{\alpha} \|L\|_{V^*}.$$

Condition (1) is often referred to as coercivity or positivity, while (2) is called continuity or boundedness. Condition 3 simply states that the right-hand side should be in the dual space of V .

In the following we will use Lax-Milgram's theorem to show that the convection-diffusion problem is well-posed. The Lax-Milgram's theorem is well-suited since it does not require symmetry of the bilinear form.

We will only consider the homogeneous Dirichlet conditions in the current argument¹. From Poincaré's lemma we know that

¹ Has the argument for reducing non-homogeneous Dirichlet conditions to homogeneous Dirichlet conditions been demonstrated elsewhere?

$$\|u\|_0 \leq C_\Omega |u|_1.$$

Using Poincare, it is straightforward to show that the semi-norm

$$|u|_1 = \left(\int (\nabla u)^2 dx \right)^{1/2}$$

and the standard H^1 norm

$$\|u\|_1 = \left(\int (\nabla u)^2 + u^2 dx \right)^{1/2}$$

are equivalent. Hence, on H_0^1 the $|\cdot|_1$ is a norm equivalent the H^1 -norm. Furthermore, this norm will be easier to use for our purposes.

For the convection-diffusion problem, we will consider two cases 1) incompressible flow, where $\nabla \cdot w = 0$ and 2) compressible flow, where $\nabla \cdot w \neq 0$. Let us for the begin with the incompressible case. Further, let

$$\begin{aligned} b(u, w) &= \int_{\Omega} \mu \nabla u \nabla w dx \\ c_w(u, w) &= \int_{\Omega} (w \cdot \nabla u) v dx \\ a(u, w) &= a(u, w) + b(u, w) \end{aligned}$$

Furthermore, assuming for the moment that $u \in H_g^1, v \in H_0^1$, we have

$$\begin{aligned} c_w(u, v) &= \int_{\Omega} w \cdot \nabla u v dx \\ &= - \int_{\Omega} w \cdot \nabla v u dx - \underbrace{\int_{\Omega} \nabla \cdot w u v dx}_{=0 \text{ (incompressibility)}} + \underbrace{\int_{\Gamma} u v w \cdot n}_{=0 \text{ (Dirichlet conditions)}} \\ &= -c_w(v, u). \end{aligned}$$

and therefore $c_w(\cdot, \cdot)$ is skew-symmetric. Letting $v = u$ we obtain that $c_w(u, u) = -c_w(u, u)$, which means that $c_w(u, u) = 0$. Therefore, the first condition in Lax-Milgram's theorem (1) is satisfied:

$$a(u, u) = b(u, u) \geq \mu |u|_1^2.$$

The second condition, the boundedness of a (2), follows by applying Cauchy-Schwartz inequality if we assume bounded flow velocities $\|v\|_\infty$.

$$\begin{aligned} a(u, v) &= \int_{\Omega} \mu \nabla u \nabla v \, dx + \int_{\Omega} (w \nabla u) v \, dx \\ &\leq \mu |u|_1 |v|_1 + \|w\|_\infty |u|_1 \|v\|_0 \\ &\leq (\mu + \|w\|_\infty C_\Omega) |u|_1 |v|_1. \end{aligned}$$

The third condition simply means that the right-hand side needs to be in the dual space of H_g^1 . Hence, we obtain the following bounds by Lax-Milgram's theorem:

$$|u|_1 \leq \frac{\mu + C_\Omega \|w\|_\infty}{\mu} \|f\|_{-1}.$$

Notice that for convection-dominated problems $C_\Omega \|w\|_\infty \gg \mu$ and the stability constant will therefore be large.

In the case where $\nabla \cdot w \neq 0$, we generally obtain that $c_w(u, u) \neq 0$. To ensure that $a(u, u)$ is still positive, we must then put some restrictions on the flow velocities. That is, we need

$$|c_w(u, u)| \leq a(u, u).$$

If $C_\Omega \|w\|_\infty \leq D\mu$ with $D < 1$ we obtain

$$\begin{aligned} a(u, u) &= \int_{\Omega} \mu \nabla u \nabla u \, dx + \int_{\Omega} (w \nabla u) u \, dx \\ &\geq \mu |u|_1 |u|_1 - \|w\|_\infty |u|_1 \|u\|_0 \\ &\geq (\mu - \|w\|_\infty C_\Omega) |u|_1 |u|_1 \\ &\geq (\mu(1 - D)) |u|_1^2. \end{aligned}$$

Further, the second condition of Lax-Milgram's theorem still applies. However, that $C_\Omega \|w\|_\infty \leq D\mu$ is clearly very restrictive compared to the incompressible case.

We remark that the Lax-Milgram conditions in the presence of the SUPG clearly will not be satisfied in the continuous case because of the third order term $-\Delta u(w \cdot \nabla v)$. With this term, the second condition of Lax-Milgram is not satisfied with $C \leq \infty$.

Finally, in order to make the term $c_w(u, u)$ skew-symmetric, it was required that the boundary integral $\int_{\Gamma} u^2 w \cdot n$ was zero. This was a consequence of the Dirichlet conditions. In general, this is neither needed nor possible at Neumann

boundaries. As long as $\int_{\Gamma} u^2 w \cdot n \geq 0$, the above argumentation is valid. From a physical point of view this means that there is outflow at the Neumann boundary, i.e., that $w \cdot n \geq 0$.

5.4 Error estimates

Finally, we provide some error estimates for the Galerkin method and the SUPG method applied to the convection-diffusion equation. Central in the derivation of both results are the following interpolation result.

Theorem 5.2 *Approximation by interpolation*

There exists an interpolation operator $I_h : H^{t+1} \rightarrow V_h$ where V_h is a piecewise polynomial field of order t with the property that for any $u \in H^t(\Omega)$

$$\|u - I_h u\|_m \leq B h^{t+1-m} \|u\|_{t+1}.$$

Proof The bounds on the interpolation error is provided by the Bramble-Hilbert lemma for $t \geq 1$ and Clement's result (the case $t = 1$), cf. e.g. [2, 3]. \square

For the Galerkin method the general and elegant result of Cea's lemma provide us with error estimates. Cea's lemma applies to general conforming approximations, i.e. when $V_h \subset V$. In our case $V = H_0^1(\Omega)$ and V_h is a finite element subspace such as for example a discretization in terms of the Lagrange elements (of any order). Hence, in our case $\|\cdot\|_V = |\cdot|_1$ and the H^1 semi-norm is equivalent with the full H^1 norm due to Poincare's inequality.

Theorem 5.3 *Cea's lemma*

Suppose the conditions for Lax-Milgram's theorem is satisfied and that we solve the linear problem (5.5) on a finite element space of order t . Then,

$$\|u - u_h\|_V \leq C_1 \frac{CB}{\alpha} h^t \|u\|_{t+1}.$$

Here $C_1 = \frac{CB}{\alpha}$, where B comes from the approximation property and α and C are the constants of Lax-Milgram's theorem.

Proof The proof is straightforward and follows from the Galerkin orthogonality:

$$a(u - u_h, v) = 0, \quad \forall v \in V_h$$

Since $V_h \subset V$:

$$\begin{aligned}
\alpha \|u - u_h\|_V^2 &\leq a(u - u_h, u - u_h) \\
&= a(u - u_h, u - v) - a(u - u_h, v - u_h) \\
&\leq C \|u - u_h\|_V \|u - v\|_V.
\end{aligned}$$

Since $v - u_h \in V_h$. Furthermore, v is arbitrary and we may therefore choose $v = I_h u$ and obtain:

$$|u - u_h|_1 \leq \frac{C}{\alpha} |u - I_h u|_1 \leq \frac{CB}{\alpha} h^t \|u\|_t,$$

where $t - 1$ is the order of the polynomials of the finite elements. \square

We remark, as mentioned above, that $\frac{C}{\alpha}$ is large for convection dominated problems and that this is what causes the poor approximation on the coarse grid, shown in Example 5.1.

To obtain improved error estimates for the SUPG method, we introduce an alternative norm:

$$\|u\|_{sd} = (h \|w \cdot \nabla u\|^2 + \mu |\nabla u|^2)^{1/2} \quad (5.8)$$

Theorem 5.4 *Suppose the conditions for Lax-Milgram's theorem is satisfied in the Hilbert space defined by the SUPG norm (5.8) and that we solve the SUPG problem (5.7) on a finite element space of order 1. Then,*

$$\|u - u_h\|_{sd} \leq Ch^{3/2} \|u\|_2$$

Proof The proof can be found in e.g. [6, 14]. \square

5.5 Exercises

Exercise 5.1 Show that the matrix obtained from a central difference scheme applied to the operator $Lu = u_x$ is skew-symmetric. Furthermore, show that the matrix obtained by linear continuous Lagrange elements are also skew-symmetric. Remark: The matrix is only skew-symmetric in the interior of the domain, not at the boundary.

Exercise 5.2 Estimate numerically the constant in Cea's lemma for various α and h for the Example 5.1.

Exercise 5.3 Implement the problem $u = \sin(\pi x)$, and $f = -\alpha u_{xx} - u_x$ and estimate numerically the constant in Cea's lemma for various α . Compare with the corresponding constant estimated from Example 5.1.

Exercise 5.4 Implement the problem $u = \sin(\pi x)$, and $f = -\alpha u_{xx} - u_x$ using SUPG and estimate the constants in the error estimate obtained by both the $|\cdot|_1$ and the $\|\cdot\|_v$ norms. Compare with the corresponding constant estimated from Example 5.1.

Exercise 5.5 Investigate whether the coersivity condition holds when a homogeneous Neumann condition is assumed on the outflow. You may assume that $v \cdot n > 0$.

Exercise 5.6 Consider the eigenvalues of the operators, L_1 , L_2 , and L_3 , where $L_1 u = u_x$, $L_2 u = -\alpha u_{xx}$, $\alpha = 1.0e^{-5}$, and $L_3 = L_1 + L_2$, with homogeneous Dirichlet conditions. For L_1 the homogeneous Dirichlet condition is enforced in $x = 0$ (since it is a first order operator) whereas for L_2 and L_3 the Dirichlet conditions are enforced in both $x = 0$ and $x = 1$. For L_3 the eigenvalue computations are mostly easily done numerically. For which of the operators are the eigenvalues positive and real?

Exercise 5.7 Compute the Sobolev norms $\|\cdot\|_m$ of the function $\sin(k\pi x)$ on the unit interval. Assume that the Sobolev norm is $\|u\|_m = (-\Delta^m u, u)^{1/2}$. What happens with negative m ? You may use either Fourier transformation or compute (eigenvalues of) powers of the stiffness matrix.

Exercise 5.8 Perform numerical experiments to determine the order of approximation with respect to various Sobolev norms and polynomial orders for the function $\sin(k\pi x)$ on the unit interval.

Chapter 6

Stokes problem

6.1 Introduction

The Stokes problem describes the flow of a slowly moving viscous incompressible Newtonian fluid. Let the fluid domain be denoted Ω . We assume that Ω is a bounded domain in \mathbb{R}^n with a smooth boundary. Furthermore, let $u : \Omega \rightarrow \mathbb{R}^n$ be the fluid velocity and $p : \Omega \rightarrow \mathbb{R}$ be the fluid pressure. The strong form of the Stokes problem can then be written as

$$-\Delta u + \nabla p = f, \text{ in } \Omega, \quad (6.1)$$

$$\nabla \cdot u = 0, \text{ in } \Omega, \quad (6.2)$$

$$u = g, \text{ on } \partial\Omega_D, \quad (6.3)$$

$$\frac{\partial u}{\partial n} - pn = h, \text{ on } \partial\Omega_N. \quad (6.4)$$

Here, f is the body force, $\partial\Omega_D$ is the Dirichlet boundary, while $\partial\Omega_N$ is the Neumann boundary. Furthermore, g is the prescribed fluid velocity on the Dirichlet boundary, and h is the surface force or stress on the Neumann boundary. These boundary condition leads to a well-posed problem provided that neither the Dirichlet nor Neumann boundaries are empty. In case of only Dirichlet conditions the pressure is only determined up to a constant, while only Neumann conditions leads to the velocity only being determined up to a constant.

These equations are simplifications of the Navier–Stokes equations for very slowly moving flow. In contrast to elliptic equations, many discretizations of this problem will lead to instabilities. These instabilities are particularly visible

as non-physical oscillations in the pressure. The following example illustrate such oscillations.

Poiseuille flow

One of the most common examples of flow problems that can be solved analytically is Poiseuille flow. It describes flow in a straight channel (or cylinder in 3D). The analytical solution is $u = (y(1-y), 0)$ and $p = 1 - x$. Since the solution is known, this flow problem is particularly useful for verifying that the code or numerical method. We therefore begin by discretizing the problem in the simplest way possible; that is, linear continuous/Lagrange elements for both velocity and pressure. The results are shown Figure 6.1. Clearly, the velocity is approximated satisfactorily, but the pressure oscillates widely and is nowhere near the actual solution.

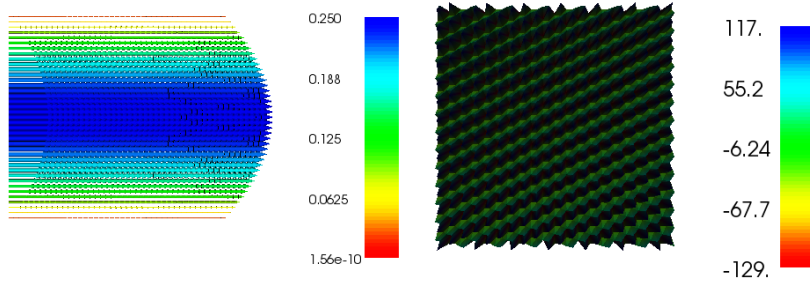


Fig. 6.1 Poiseuille flow solution obtained with linear continuous elements for both velocity and pressure. The left figure shows the (well-represented) velocity while the right shows the pressure (with the wild oscillations).

```
from dolfin import *

def u_boundary(x):
    return x[0] < DOLFIN_EPS or x[1] > 1.0 - DOLFIN_EPS or x[1]
        < DOLFIN_EPS

def p_boundary(x):
    return x[0] > 1.0 - DOLFIN_EPS

mesh = UnitSquare(40,40)
```

```

V = VectorFunctionSpace(mesh, "Lagrange", 1)
Q = FunctionSpace(mesh, "Lagrange", 1)
#Q = FunctionSpace(mesh, "DG", 0)
W = MixedFunctionSpace([V, Q])

u, p = TrialFunctions(W)
v, q = TestFunctions(W)

f = Constant([0,0])

u_analytical = Expression(["x[1]*(1-x[1])", "0.0"])
p_analytical = Expression("-2+2*x[0]")

bc_u = DirichletBC(W.sub(0), u_analytical, u_boundary)
bc = [bc_u]

a = inner(grad(u), grad(v))*dx + div(u)*q*dx + div(v)*p*dx
L = inner(f, v)*dx

UP = Function(W)
A, b = assemble_system(a, L, bc)
solve(A, UP.vector(), b, "lu")

U, P = UP.split()

plot(U, title="Numerical velocity")
plot(P, title="Numerical pressure")

U_analytical = project(u_analytical, V)
P_analytical = project(p_analytical, Q)

plot(U_analytical, title="Analytical velocity")
plot(P_analytical, title="Analytical pressure")

interactive()

```

However, when using the second order continuous elements for the velocity and first order continuous elements for the pressure, we obtain the perfect solution shown in Figure 6.2.

The previous example demonstrates that discretizations of the Stokes problem may lead to, in particular, strange instabilities in the pressure. In this chapter we will describe why this happens and several strategies to circumvent this behaviour.

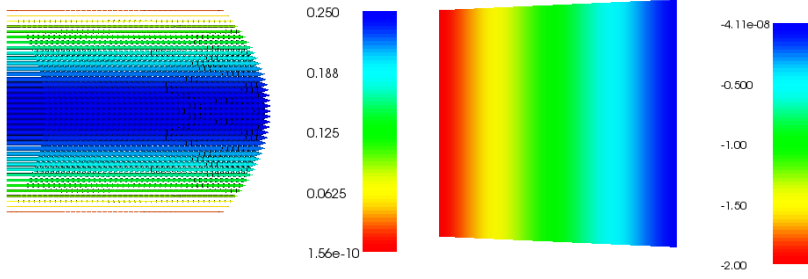


Fig. 6.2 Poiseuille flow solution obtained with quadratic continuous elements for the velocity and linear continuous elements for the pressure. The left figure shows the velocity while the right shows the pressure. Both the velocity and the pressure are correct.

6.2 Finite Element formulation

Let us first start with a weak formulation of Stokes problem: Find $u \in H_{D,g}^1$ and $p \in L^2$.

$$\begin{aligned} a(u, v) + b(p, v) &= f(v), \quad v \in H_{D,0}^1 \\ b(q, u) &= 0, \quad q \in L^2, \end{aligned}$$

where

$$\begin{aligned} a(u, v) &= \int \nabla u : \nabla v \, dx, \\ b(p, v) &= \int p \nabla \cdot v \, dx, \\ f(v) &= \int f v \, dx + \int_{\Omega_N} h v \, ds. \end{aligned}$$

Here $H_{D,g}^1$ contains functions in H^1 with trace g on $\partial\Omega_D$. To obtain symmetry we have substituted $\hat{p} = -p$ for the pressure and is referint to \hat{p} as p .

As before the standard finite element formulation follows directly from the weak formulation: Find $u_h \in V_{g,h}$ and $p_h \in Q_h$ such that

$$a(u_h, v_h) + b(p_h, v_h) = f(v_h), \quad \forall v_h \in V_{0,h}, \quad (6.5)$$

$$b(q_h, u_h) = 0, \quad \forall q_h \in Q_h. \quad (6.6)$$

Letting $u_h = \sum_{i=1}^n u_i N_i$, $p_h = \sum_{i=1}^m p_i L_i$, $v_h = N_j$, and $q_h = L_j$ we obtain a linear system on the form

$$\begin{bmatrix} A & B^T \\ B & 0 \end{bmatrix} \begin{bmatrix} u \\ p \end{bmatrix} = \begin{bmatrix} f \\ 0 \end{bmatrix} \quad (6.7)$$

Here

$$A_{ij} = a(N_i, N_j) = \int \nabla N_i \nabla N_j \, dx, \quad (6.8)$$

$$B_{ij} = b(L_i, N_j) = \int \nabla L_i N_j \, dx. \quad (6.9)$$

Hence, A is $n \times n$, while B is $m \times n$, where n is the number of degrees of freedom for the velocity field, while m is the number of degrees of freedom for the pressure.

Is the system (6.7) invertible? For the moment, we assume that the submatrix A is invertible. This is typically the case for Stokes problem. We may then perform blockwise Gauss elimination: That is, we multiply the first equation with A^{-1} to obtain

$$u = A^{-1}f - A^{-1}B^T p$$

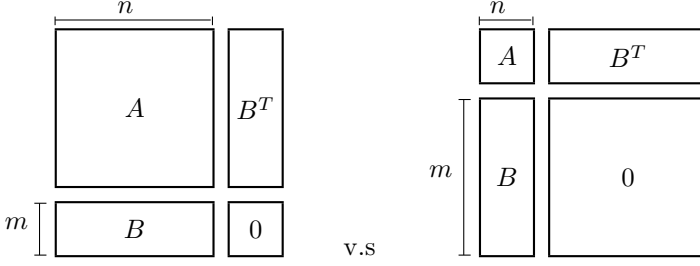
Then, we then insert u in the second equation to get

$$0 = Bu = BA^{-1}f - BA^{-1}B^T p$$

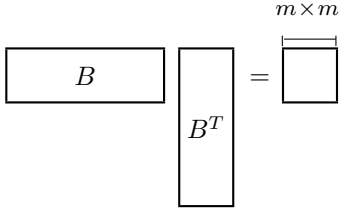
i.e we have removed v and obtained an equation only involving p :

$$BA^{-1}B^T p = BA^{-1}f$$

This equation is often called the pressure Schur complement. The question is then reduced to whether $BA^{-1}B^T$ is invertible. Consider the following two situations:



Clearly, the right most figure is not invertible since $n \ll m$ and the 0 in the lower right corner dominates. For the left figure one might expect that the matrix is non-singular since $n \gg m$, but it will depend on A and B . We have already assumed that A is invertible, and we therefore ignore A^{-1} in $BA^{-1}B^T$. The question is then whether BB^T is invertible.



As illustrated above, BB^T will be a relatively small matrix compared to B^T and A as long as $n \gg m$. Therefore, BB^T may therefore be non-singular. To ensure that BB^T is invertible, it is necessary that

$$\text{kernel}(B^T) = 0, \text{ where } B \text{ is } m \times n$$

An equivalent statement is that

$$\max_v (v, B^T p) > 0 \quad \forall p. \quad (6.10)$$

Alternatively,

$$\max_v \frac{(v, B^T p)}{\|v\|} \geq \beta \|p\| \quad \forall p. \quad (6.11)$$

which obviously may be written

$$\max_v \frac{(Bv, p)}{\|v\|} \geq \beta \|p\| \quad \forall p. \quad (6.12)$$

Here, $\beta > 0$. We remark that (6.10) and (6.11) are equivalent for a finite dimensional matrix. However, in the infinite dimensional setting of PDEs (6.10) and (6.11) are different. Inequality (6.10) allow $(v, B^T p)$ to approach zero, while (6.11) requires a lower bound. For the Stokes problem, the corresponding condition is crucial:

$$\sup_{v \in H_{D,g}^1} \frac{(p, \nabla \cdot u)}{\|u\|_1} \geq \beta \|p\|_0 > 0, \quad \forall p \in L^2 \quad (6.13)$$

Similarly, to obtain order optimal convergence rates, that is

$$\|u - u_h\|_1 + \|p - p_h\|_0 \leq Ch^k \|u\|_{k+1} + Dh^{\ell+1} \|p\|_{\ell+1}$$

where k and ℓ are the ploynomial degree of the velocity and the pressure, respectively, the celebrated *Babuska-Brezzi condition* has to be satisfied:

$$\sup_{v \in V_{h,g}} \frac{(p, \nabla \cdot v)}{\|v\|_1} \geq \beta \|p\|_0 > 0, \quad \forall p \in Q_h \quad (6.14)$$

We remark that the discrete condition (6.14) does not follow from (6.13). In fact, it has been a major challenge in numerical analysis to determine which finite element pairs V_h and Q_h that meet this condition.

Remark 6.1 For saddle point problems on the form (6.5)-(6.6) four conditions have to be satisfied in order to have a well-posed problem:

Boundedness of a :

$$a(u_h, v_h) \leq C_1 \|u_h\|_{V_h} \|v_h\|_{V_h}, \quad \forall u_h, v_h \in V_h, \quad (6.15)$$

and boundedness of b :

$$b(u_h, q_h) \leq C_2 \|u_h\|_{V_h} \|q_h\|_{Q_h}, \quad \forall u_h \in V_h, q_h \in Q_h, \quad (6.16)$$

Coersivity of a :

$$a(u_h, u_h) \geq C_3 \|u_h\|_{V_h}^2, \quad \forall u_h \in Z_h, \quad (6.17)$$

where $Z_h = \{u_h \in V_h \mid b(u_h, q_h) = 0, \forall q_h \in Q_h\}$ and "coersivity" of b :

$$\sup_{u_h \in V_h} \frac{b(u_h, q_h)}{\|u_h\|_{V_h}} \geq C_4 \|q_h\|_{Q_h}, \quad \forall q_h \in Q_h. \quad (6.18)$$

For the Stokes problem, (6.15)-(6.17) are easily verified, while (6.18) often is remarkably difficult unless the elements are designed to meet this condition. We remark also that condition (6.17) strictly speaking only needs to be valid on a subspace of V_h but this is not important for the Stokes problem.

6.3 Examples of elements

6.3.1 The Taylor-Hood element

The Taylor-Hood elements are quadratic for the velocity and linear for pressure, i.e., the i 'th basis function of the velocity and pressure are of the form

$$\begin{aligned} u : N_i &= a_i + b_i x + c_i y + d_i xy + e_i x^2 + f_i y^2, \\ p : L_i &= k_i + l_i x + m_i y. \end{aligned}$$

And the basis functions are continuous across elements. For the Taylor-Hood element we have the following error estimate:

$$\|u - u_h\|_1 + \|p - p_h\|_0 \leq Ch^2(\|u\|_3 + \|p\|_2).$$

The generalization of the Taylor-Hood element to higher order, that is $P_k - P_{k-1}$, satisfies the Brezzi conditions (on reasonable meshes). For the Taylor-Hood element of higher order we have the following error estimate:

$$\|u - u_h\|_1 + \|p - p_h\|_0 \leq Ch^k(\|u\|_{k+1} + \|p\|_k).$$

6.3.2 The Crouzeix-Raviart element

This element is linear in velocity and constant in pressure. Hence, the i 'th basis functions are of the form:

$$\begin{aligned} v : N_i &= a_i + b_i x + c_i y \\ p : L_i &= a_i \end{aligned}$$

The v element is continuous *only* in the mid-point of each side, and the p element is discontinuous. The Crouzeix-Raviart element satisfies the inf-sup

condition, but is non-conforming because it is only continuous at the mid-point of each element. The non-conformity does not affect the approximation properties for the Stokes problem, but can not be used if the $-\Delta u - \nabla p = f$ is replaced with the more "physically correct" $-\nabla \cdot \epsilon(u) - \nabla p = f$, where $\epsilon = \frac{1}{2}(\nabla + \nabla^T)$ is the symmetric gradient. For the Crouzeix–Raviart element we have the following error estimate:

$$\|u - u_h\|_1 + \|p - p_h\|_0 \leq Ch(\|u\|_2 + \|p\|_1)$$

The element may be generalized to odd, but not even orders.

6.3.3 The P1-P0 element

The P1-P0 element is perhaps the most natural element to consider as it consists of combining continuous piecewise linear functions for the velocity with piecewise constants for the pressure. This combination often work quite well, and this puzzled the community for quite some time. However, this combination is not inf-sup stable and oscillations in the pressure may occur.

6.3.4 The P2-P0 element

$P_2 - P_0$ element is a popular element that satisfies the Brezzi conditions. An advantage with this approach is that mass conservation is maintained elementwise. However, the approximation properties of the pressure is one order lower than that for the Taylor-Hood element and consequently the velocity approximation is also formally, in general, reduced by one order, i.e.,

$$\|u - u_h\|_1 + \|p - p_h\|_0 \leq C_0 h^2 \|u\|_2 + C_1 h \|p\|_2$$

The $P_2 - P_0$ element can be generalized to higher order. In fact, $P_k - P_{k-2}$, satisfies the Brezzi conditions for $k \geq 2$. Here, the pressure element P_{k-2} may in fact consist of both continuous and discontinuous polynomials. The discontinuous polynomials then has the advantage of providing mass conservation, albeit at the expanse of many degrees of freedom compared with the continuous variant.

6.3.5 The Mini element

The mini element is linear in both velocity and pressure, but with one degree of freedom added per element since it is well-known that elements that are linear in both v and p will not satisfy the inf-sup condition. The extra degree of freedom is in 2D constructed such it is a cubic polynomial which is zero at all element faces. For example, on the reference element, the barycentric coordinates x , y , and $1 - x - y$ are all zero at their respective faces. Hence, the composition $xy(1 - x - y)$ is zero at all element faces. The barycentric coordinates can be used for this purpose on any element and also in higher dimensions. The function is often called the bubble function as its support is local to one element and is zero at the element faces. For the Mini element we have the following error estimate:

$$\|u - u_h\|_1 + \|p - p_h\|_0 \leq C_0 h \|u\|_2 + C_1 h^2 \|p\|_2$$

We notice that the convergence rate for the velocity is linear, hence the extra bubbles bring stability but does not increase approximation order.

6.4 Stabilization techniques to circumvent the Babuska-Brezzi condition

Stabilization techniques typically replace the system:

$$\begin{aligned} Au + B^T p &= f \\ Bu &= 0 \end{aligned}$$

with an alternative system

$$\begin{aligned} Au + B^T p &= f \\ Bu - \epsilon Dp &= \epsilon d, \end{aligned}$$

where ϵ is properly chosen and D is a positive, but not necessarily positive definite, matrix.

To see that we obtain a nonsingular system we again multiply the first equation with A^{-1} and then factorize:

$$\begin{aligned}
u &= A^{-1}f - A^{-1}B^T p \\
Bu &= BA^{-1}f - BA^{-1}B^T p = \epsilon d + \epsilon Dp \\
(BA^{-1}B^T + \epsilon D)p &= BA^{-1}f - \epsilon d
\end{aligned}$$

If D is nonsingular then $(BA^{-1}B^T + \epsilon D)$ will be nonsingular since both D and $BA^{-1}B^T$ are positive (only D is positive definite however).

Factorizing for p we end up with a *Velocity-Schur complement*. Solving for p in the second equation and inserting the expression for p into the first equation we have

$$\begin{aligned}
p &= (-\epsilon D)^{-1}(\epsilon d - Bu) \\
&\Downarrow \\
Au + B^T(-\epsilon D)^{-1}(\epsilon d - Bu) &= f \\
(A + \frac{1}{\epsilon}B^T D^{-1}B)u &= f + D^{-1}d
\end{aligned}$$

$(A + \frac{1}{\epsilon}B^T D^{-1}B)$ is nonsingular since A is nonsingular and $B^T D^{-1}B$ is positive.

At least, three techniques have been proposed for stabilization. These are:

1. $\nabla \cdot v + \epsilon \Delta p = 0$. Pressure stabilization. Motivated through mathematical intuition (from the convection-diffusion equation).
2. $\nabla \cdot v - \epsilon p = 0$. Penalty method. Typically, one uses the Velocity-Schur complement
3. $\nabla \cdot -\epsilon \frac{\partial p}{\partial t} = 0$. Artificial compressibility. A practical method as one adds the possibility for time stepping.

In other words, these techniques sets D to be

1. $D = A$
2. $D = M$
3. $D = \frac{1}{\Delta t}M$

where A is the stiffness matrix (discrete laplace operator) and M is the mass matrix.

6.5 Exercises

Exercise 6.1 Show that the conditions (6.15)-(6.17) are satisfied for $V_h = H_0^1$ and $Q_h = L^2$.

Exercise 6.2 Show that the conditions (6.15)-(6.17) are satisfied for Taylor–Hood and Mini discretizations. (Note that Crouzeix–Raviart is non-conforming so it is more difficult to prove these conditions for this case.)

Exercise 6.3 Condition (6.18) is difficult to prove. However, if we assume that $V_h = L^2$ and $Q_h = H_0^1$, you should be able to prove it. (Hint: This is closely related to Poincaré’s inequality.)

Exercise 6.4 Test other finite elements for the Poiseuille flow problem. Consider $P_1 - P_0$, $P_2 - P_2$, $P_2 - P_0$, as well as the Mini and Crouzeix–Raviart element.

Exercise 6.5 Implement stabilization for the Poiseuille flow problem and use first order linear elements for both velocity and pressure.

Exercise 6.6 In the previous problem the solution was a second order polynomial in the velocity and first order in the pressure. We may therefore obtain the exact solution and it is therefore difficult to check order of convergence for higher order methods with this solution. In this exercise you should therefore implement the problem $u = (\sin(\pi y), \cos(\pi x))$, $p = \sin(2\pi x)$, and $f = -\Delta u - \nabla p$. Test whether the approximation is of the expected order for $P_4 - P_3$, $P_4 - P_2$, $P_3 - P_2$, and $P_3 - P_1$.

Exercise 6.7 Implement the Stokes problem with analytical solution $u = (\sin(\pi y), \cos(\pi x))$, $p = \sin(2\pi x)$, and $f = -\Delta u - \nabla p$ on the unit square. Consider the case where you have Dirichlet conditions on the sides ‘x=0’, ‘x=1’ and ‘y=1’ while Neumann is used on the last side (this way we avoid the singular system associated with either pure Dirichlet or pure Neumann problems). Then determine the order of the approximation of wall shear stress on the side ‘x=0’. The wall shear stress on the side ‘x=0’ is $\nabla u \cdot t$ where $t = (0, 1)$ is the tangent along ‘x=0’.

Chapter 7

Efficient Solution Algorithms: Iterative methods and Preconditioning

To compute the solution of a partial differential equation, we often need to solve a system of linear equations with a large number of unknowns. The accuracy of the solution increases with the number of unknowns used. Nowadays, unknowns in the order of millions to billions are routinely solved for without the use of (state-of-the-art) high-performance computing. Such computations are facilitated by the enormous improvements in numerical algorithms and scientific software the last decades.

It should be quite clear that naive Gaussian elimination can not be employed. For a naive Gaussian elimination implementation, the number of required floating point operations (FLOPS) scales as the cube of the number of unknowns. Hence, solving a problem with 10^6 unknowns would then require 10^{18} FLOPS which on a modern computer with e.g. 3 GHz still would take about 10 years. As we will see later, such problems may in common cases be solved in just a few seconds. There are two ingredients in such efficient algorithms: *iterative methods* and *preconditioning*.

Lets therefore consider the numerical solution of large linear systems,

$$Au = b,$$

where the linear system comes from discretization of PDEs. That is, A is a $N \times N$ matrix, and N is between 10^6 and 10^9 in typical simulations. Furthermore, the matrix is normally extremely sparse and contains only $\mathcal{O}(N)$ nonzeros (see Exercise 7.1). It is important to notice that even though A is sparse A^{-1} will in general be full. This is a main reason to consider iterative methods.

7.1 The simplest iterative method: the Richardson iteration

The Richardson iteration¹ is

$$u^n = u^{n-1} - \tau(Au^{n-1} - b), \quad (7.1)$$

where τ is a relaxation parameter that must be determined. Clearly, the method is consistent in the sense that if $u^{n-1} = u$, then $u^n = u$ and the iterative method has converged to the exact solution. It is also clear that each iteration requires the evaluation of A on a vector, in addition to vector addition and scalar multiplication. Hence, one iteration requires the amount of $\mathcal{O}(N)$ FLOPS and only $\mathcal{O}(N)$ of memory. This is a dramatic improvement when compared Gaussian elimination at least if the number of iterations are few. The key to obtain few iterations is preconditioning, but let's first consider the Richardson's method without.

The standard approach to analyze iterative methods is to look at what happens with the *error*. Let the error at the n 'th iteration be $e^n = u^n - u$. As this is a linear system of equations, we may subtract u from both sides of (7.1) and obtain an equation for the iterative error:

$$e^n = e^{n-1} - \tau Ae^{n-1}.$$

We may therefore quantify the error in terms of the L^2 -norm as

$$\|e^n\| = \|e^{n-1} - \tau Ae^{n-1}\| \leq \|I - \tau A\| \|e^{n-1}\|.$$

Clearly, if $\|I - \tau A\| < 1$ then the iteration will be convergent.

Assuming for the moment that A is symmetric and positive definite, then the norm of A in general defined as

¹ Richardson developed his method prior to computers. In his 1910 paper, where the focus is to predict stresses in a masonry dam, he describes how he uses humans as computational resources. He writes "So far I have paid piece rates for the operation [Laplacian] of about $n/18$ pence per coordinate point, n being the number of digits. As for the rate of working, one of the quickest boys average 2000 operations per week, for numbers of three digits, those done wrong being discounted."

$$\|A\| = \max_x \frac{\|Ax\|}{\|x\|}$$

equals the largest eigenvalue of A , λ_{max} . Furthermore, if we assume that the eigenvalues are ordered with respect to increasing value, such that λ_0 and λ_N are the smallest and largest eigenvalue, then the norm of $I - \tau A$,

$$\|I - \tau A\| = \max_x \frac{\|(I - \tau A)x\|}{\|x\|}$$

is attained either for the smallest or largest eigenvalue as either $(1 - \tau\lambda_0)$ or $-(1 - \tau\lambda_N)$. The optimal relaxation parameter τ_{opt} can be stated in terms of the eigenvalues, λ_i , of A . Minimum is attained when $(1 - \tau_{opt}\lambda_0) = -(1 - \tau_{opt}\lambda_N)$ which makes $\tau_{opt} = \frac{2}{\lambda_0 + \lambda_N}$.

Let the convergence factor ρ be defined as

$$\rho = \|I - \tau A\|$$

The convergence factor with an optimal relation is then

$$\rho = \|I - \tau A\| = \max_{\lambda_i} |1 - \tau\lambda_i| = 1 - \tau\lambda_0 = 1 - \frac{2\lambda_0}{\lambda_0 + \lambda_N} = \frac{\lambda_N - \lambda_0}{\lambda_N + \lambda_0} = \frac{\kappa - 1}{\kappa + 1}.$$

Here, $\kappa = \frac{\lambda_N}{\lambda_0}$ is the condition number.

We estimate the error reduction per iteration in terms of the convergence factor as,

$$\|e^n\| = \|(I - \tau A)e^{n-1}\| \leq \rho\|e^{n-1}\|.$$

which leads to

$$\|e^n\| \leq \left(\frac{\kappa - 1}{\kappa + 1}\right)^n \|e^0\|.$$

For iterative methods, we never iterate until the true solution exactly. Instead a convergence criteria needs to be chosen such that the error obtained by the iterative method is less than or at least comparable to the approximation error of the original system. Determining an appropriate convergence criteria is problem dependent and quite often challenging.

Nevertheless, let us assume that we need to reduce the error by a factor of ϵ , that is, we need $\frac{\|e^n\|}{\|e^0\|} < \epsilon$. From the iteration, we have

$$\|e^n\| \leq \rho\|e^{n-1}\| \leq \rho^n\|e^0\|. \quad (7.2)$$

An estimate for the number of iterations is then obtained by assuming equality in the equation (7.2) and $\frac{\|e^n\|}{\|e^0\|} = \epsilon$. Then the number of iterations needed to achieve the desired error is:

$$n = \frac{\log \epsilon}{\log \rho} = \frac{\log \epsilon}{\log(\frac{K-1}{K+1})}. \quad (7.3)$$

If n is independent of the resolution of the discretization, the computational cost of the algorithm is $\mathcal{O}(N)$ in FLOPS and memory and the algorithm is *order-optimal*.

The current analysis of the simplest iterative method there is, the Richardson iteration, shows that the efficiency of the method is determined by the condition number of the matrix. In the literature you will find a jungle of methods of which the following are the most famous: the Conjugate Gradient method, the Minimal Residual method, the BiCGStab method, and the GMRES method. It is remarkable that in general the convergence of these methods is determined by the condition number with one exception; the Conjugate Gradient method which often can be estimated in terms of the square root of the condition number. One main advantage is however that these methods do not require the determination of a τ to obtain convergence.

Eigenvalues of an elliptic problem in 1D and 2D.

Let us consider an elliptic problem:

$$u - \Delta u = f, \quad \text{in } \Omega, \quad (7.4)$$

$$\frac{\partial u}{\partial n} = 0, \quad \text{on } \partial\Omega. \quad (7.5)$$

Notice that the lower order term u in front of $-\Delta u$ makes removes the singularity associated with Neumann conditions and that in the continuous case the smallest eigenvalue is 1 (associated with the eigenfunction that is a constant throughout Ω). The following code computes the eigenvalues using linear Lagrangian elements and

```
from dolfin import *
from numpy import linalg

for D in [1, 2]:
    for N in [4, 8, 16, 32]:
```

```

if D == 1: mesh = UnitIntervalMesh(N)
elif D == 2: mesh = UnitSquareMesh(N, N)

V = FunctionSpace(mesh, "Lagrange", 1)
u = TrialFunction(V)
v = TestFunction(V)

a = u*v*dx + inner(grad(u), grad(v))*dx
A = assemble(a)
e = linalg.eigvals(A.array())
e.sort()
c = e[-1] / e[0]

print "D=%d, N=%3d, min eigenvalue=%5.3f, max
      eigenvalue=%5.3f, cond.
      number=%5.3f " % (D, N, e
[0], e[-1], c)

```

yields the following output:

```

D=1, N= 4, min eig=0.199, max eig=14.562, cond. number=73.041
D=1, N= 8, min eig=0.111, max eig=31.078, cond. number=279.992
D=1, N= 16, min eig=0.059, max eig=63.476, cond.
number=1079.408
D=1, N= 32, min eig=0.030, max eig=127.721, cond.
number=4215.105
D=2, N= 4, min eig=0.040, max eig=7.090, cond. number=178.444
D=2, N= 8, min eig=0.012, max eig=7.735, cond. number=627.873
D=2, N= 16, min eig=0.003, max eig=7.929, cond. number=2292.822
D=2, N= 32, min eig=0.001, max eig=7.982, cond. number=8693.355

```

The output shows that the condition number grows as h^{-2} in both 1D and 2D although the behaviour of the eigenvalues clearly are dimension dependent (see Exercise 7.2). The smallest eigenvalue decrease in both 1D and 2D as $h \rightarrow 0$ but at different rates. To obtain eigenvalues corresponding the true eigenvalue we would need to solve a generalized eigenvalue problem as discussed in Chapter 2.

The Richardson iteration applied to a 1D Poisson equation.

The Richardson iteration on the Poisson equation in 1D, discretized with finite difference method (FDM).

$$Lu = \begin{cases} -u'' = f & \text{for } x \in (0, 1) \\ u(0) = u(1) = 0 \end{cases} \quad (7.6)$$

Eigenvalues and eigenfunctions of Lu are $\lambda_k = (k\pi)^2$ and $v_k = \sin(k\pi x)$ for $k \in \mathbb{N}$. When discretizing with FDM we get a $Au = b$ system, where A is a tridiagonal matrix ($A = \text{tridiagonal}(-1, 2, -1)$) when the Dirichlet conditions have been eliminated. The discrete and continuous eigenvectors are the same, but the eigenvalues are a little bit different: $\lambda_k = \frac{4}{h^2} \sin^2(\frac{k\pi h}{2})$, where h is the step length Δx . We find the smallest and largest discrete eigenvalues

$$\lambda_{\min}(A) = \pi^2, \quad \lambda_{\max}(A) = \frac{4}{h^2}.$$

Let $\tau = \frac{2}{\lambda_{\max} + \lambda_{\min}}$ then from the analysis above,

$$\|e^n\| \leq \left(\frac{1-K}{1+K}\right)^n \|e^0\|.$$

The below code perform the Richardson iteration for various resolution on the 1D Poisson problem and stops when the convergence criteria $\frac{\|r_k\|}{\|r_0\|} \leq 10^{-6}$ is obtained.

```
from numpy import *

def create_stiffness_matrix(N):
    h = 1.0/(N-1)
    A = zeros([N,N])
    for i in range(N):
        A[i,i] = 2.0/(h**2)
        if i > 0:
            A[i,i-1] = -1.0/(h**2)
        if i < N-1:
            A[i,i+1] = -1.0/(h**2)
    A = matrix(A)
    return A

Ns = [10, 20, 40, 80, 160, 320]
for N in Ns:
    A = create_stiffness_matrix(N) # creating
                                   matrix
```

```

x = arange(0, 1, 1.0/(N))
f = matrix(sin(3.14*x)).transpose()           # right hand
                                              side
u0 = matrix(random.random(N)).transpose()      # initial guess
u_prev = u0

eigenvalues = sort(linalg.eigvals(A))          # compute
                                              eigenvalues and tau
lambda_max, lambda_min = eigenvalues[-1], eigenvalues[0]
print "lambda_max ", lambda_max, " lambda_min ", lambda_min
tau = 2/(lambda_max + lambda_min)

norm_of_residual = 1.0                        # make sure the
                                              iteration starts
no_iterations = 0
while norm_of_residual > 1.0e-6:
    r = A*u_prev - f                          # compute the
                                              residual
    u = u_prev - tau*r                        # the Richardson
                                              iteration
    u_prev = u
    norm_of_residual = r.transpose()*r         # check for norm
                                              of residual
    no_iterations += 1                         # count no
                                              iterations

print "N ", N, " number of iterations ", no_iterations

```

N	λ_{min}	λ_{max}	no. iterations	Estimated FLOPS
10	6.6	317	277	$11 \cdot 10^3$
20	8.1	1435	1088	$87 \cdot 10^3$
40	8.9	6075	4580	$732 \cdot 10^3$
80	9.4	$25 \cdot 10^3$	$20 \cdot 10^3$	$6.4 \cdot 10^6$
160	9.6	$101 \cdot 10^3$	$84 \cdot 10^3$	$53 \cdot 10^6$
320	9.7	$407 \cdot 10^3$	$354 \cdot 10^3$	$453 \cdot 10^6$

Table 7.1 The number of iterations of the Richardson iteration for solving a 1D Poisson problem. The FLOPS is estimated as the number of iterations times four times the number of unknowns, N , as the matrix is tridiagonal and there is both a matrix vector product ($3N$) and a vector addition involved in (7.1).

We remark that in this example we have initialized the iteration with a random vector because such a vector contains errors at all frequencies. This is recommended practice when trying to establish a worst case scenario. Testing

the iterative method against a known analytical solution with a zero start vector will often only require smooth error to be removed during the iterations and will therefore underestimate the complications of a real-world problem.

7.1.1 The stopping criteria

In the Example 7.1 we considered the Richardson iteration applied to a Poisson problem in 1D. We saw that in order to stop the iteration we had to choose a stopping criteria. Ideally we would like to stop when the error was small enough. The problem is that the error is unknown. In fact, since $e^n = u^n - u$ we would be able to compute the exact solution if the error was known at the n 'th iteration. What is computable is the *residual* at the n 'th iteration, defined by

$$r^n = Au^n - f.$$

It is straightforward to show that

$$Ae^n = r^n.$$

But computing e^n from this relation would require the inversion of A (which we try to avoid at all cost since it in general is a $\mathcal{O}(N^3)$ procedure). For this reason, the convergence criteria is typically expressed in terms of some norm of the residual. We may bound the n 'th error as

$$\|e^n\| \leq \|A^{-1}\| \|r^n\|.$$

However, estimating $\|A^{-1}\|$ is in general challenging or computationally demanding and therefore usually avoided. To summarize, choosing an appropriate stopping criteria is in general challenging and in practice the choice has to be tailored to concrete application at hand by trial and error.

7.2 The idea of preconditioning

The basic idea of preconditioning is to replace

$$Au = b$$

with

$$BAu = Bb.$$

Both systems have the same solution (if B is nonsingular). However, B should be chosen as a cheap approximation of A^{-1} or at least in such a way that BA has a smaller condition number than A . Furthermore Bu should cost $\mathcal{O}(N)$ operations to evaluate. Obviously, the preconditioner $B = A^{-1}$ would make the condition number of BA be one and the Richardson iteration would converge in one iteration. However, $B = A^{-1}$ is a very computationally demanding preconditioner. We would rather seek preconditioners that are $\mathcal{O}(N)$ in both memory consumption and evaluation.

The generalized Richardson iteration becomes

$$u^n = u^{n-1} - \tau B(Au^{n-1} - b). \quad (7.7)$$

The error in the n -th iteration is

$$e^n = e^{n-1} - \tau BAe^{n-1}$$

and the iteration is convergent if $\|I - \tau BA\| < 1$.

7.2.1 Spectral equivalence and order optimal algorithms

Previously we stated that a good preconditioner is supposed to be similar to A^{-1} . The precise (and most practical) property that is required of a preconditioner is:

- B should be spectrally equivalent with A^{-1} .
- The evaluation of B on a vector, Bv , should be $\mathcal{O}(N)$.
- The storage of B should be $\mathcal{O}(N)$.

Definition 7.1 Two linear operators or matrices A^{-1} and B , that are symmetric and positive definite are spectral equivalent if:

$$c_1(A^{-1}v, v) \leq (Bv, v) \leq c_2(A^{-1}v, v) \quad \forall v \quad (7.8)$$

If A^{-1} and B are spectral equivalent, then the condition number of the matrix BA is $\kappa(BA) \leq \frac{c_2}{c_1}$.

If the preconditioner B is spectrally equivalent with A^{-1} then the preconditioned Richardson iteration yields an order optimal algorithm. To see this, we note that $e^n = (I - \tau BA)e^{n-1}$. We can estimate the behavior of e^n by using the A -norm, $\rho_A = \|I - \tau BA\|_A$. Then we get

$$\|e^n\|_A \leq \rho_A \|e^{n-1}\|_A.$$

Hence, if the condition number is independent of the discretization then the number of iterations as estimated earlier in (7.3) will be bounded independently of the discretization.

In general, if A is a discretization of $-\Delta$ on a quasi-uniform mesh then both multigrid methods and domain decomposition methods will yield preconditioners that are spectrally equivalent with the inverse and close to $\mathcal{O}(N)$ in evaluation and storage. The gain in using a proper preconditioner may provide speed-up of several orders of magnitude, see Example 7.3.

7.3 Krylov methods and preconditioning

For iterative methods, any method involving linear iterations may be written as a Richardson iteration with a preconditioner. However, iterative methods like Conjugate Gradient method, GMRES, Minimal Residual method, and BiCGStab, are different. These are nonlinear iterations where for instance the relaxation parameter τ changes during the iterations and are in fact often chosen optimally with respect to the current approximation. Avoiding the need to determine a fixed relaxation parameter prior to the iterations is of course a huge practical benefit. Still, the convergence in practice can usually be roughly estimated by the convergence analysis above for the Richardson iteration.

We will not go in detail on these methods. We only remark that also with these methods it is essential with a good preconditioning technique in order for efficient computations. Furthermore, some of them have special requirements and in some cases it is well-known what to use.

General Advice for usage of different methods:

We classify the methods according to the matrices they are used to solve.

- If a matrix is Symmetric Positive Definite (SPD), i.e., $A = A^T$ and $x^T Ax \geq 0 \forall x$ the *Conjugate Gradient method* (CG) is the method of choice. CG needs an SPD preconditioner, see also Exercise 7.6.
- If a matrix is Symmetric but indefinite, i.e. $A = A^T$ but both positive and negative eigenvalues then the *Minimal Residual method* (MR) is the best choice. MR requires an SPD preconditioner, see also Exercise 7.9.
- If the matrix is positive, i.e., $x^T Ax \geq 0 \forall x$ which is often the case for convection-diffusion problems or flow problems then *GMRES* with either ILU or AMG are often good, but you might need to experiment, see also Exercise 7.7.
- For matrices that are both nonsymmetric and indefinite there is a jungle of general purpose methods but they may be categorized in two different families. In our experience the *BiCGStab* and *GMRES* methods are the two most prominent algorithms in these families. *GMRES* is relatively robust but may stagnate. *BiCGStab* may break down. *GMRES* has a parameter 'the number of search vectors' that may be tuned.

Most linear algebra libraries for high performance computing like for instance PETSc, Trilinos, Hypr have these algorithms implemented. They are also implemented in various libraries in Python and Matlab. There is usually no need to implement these algorithms yourself.

[

CPU times of different algorithms] In this example we will solve the problem

$$\begin{aligned} u - \Delta u &= f, & \text{in } \Omega \\ \frac{\partial u}{\partial n} &= 0, & \text{on } \partial\Omega \end{aligned}$$

where Ω is the unit square with first order Lagrange elements. The problem is solved with four different methods:

- a LU solver,
- Conjugate Gradient method,
- Conjugate Gradient method with an ILU preconditioner, and
- Conjugate Gradient method with an AMG preconditioner,

for $N = 32^2, 64^2, 128^2, 256^2, 512^2, 1024^2$, where N is the number of degrees of freedom.

Figure 7.1 shows that there is a dramatic difference between the algorithms. In fact the Conjugate gradient (CG) with an AMG preconditioner is over 20 times

faster than the slowest method, which is the CG solver without preconditioner. One might wonder why the LU solver is doing so well in this example when it costs $\mathcal{O}(N^2) - \mathcal{O}(N^3)$. However, if we increase the number of degrees of freedom, then the method would slow down compared to the other methods. The problem is then that it would require too much memory and the program would probably crash.

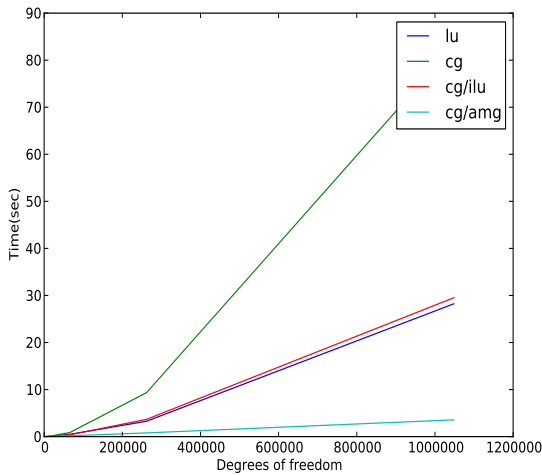


Fig. 7.1 CPU time (in seconds) for solving a linear system of equation with N degrees of freedom (x-axis) for different solvers

```
from dolfin import *
import time
lu_time = []; cgamg_time = []
cg_time = []; cgilu_time = []
Ns = []

parameters["krylov_solver"]["relative_tolerance"] = 1.0e-8
parameters["krylov_solver"]["absolute_tolerance"] = 1.0e-8
parameters["krylov_solver"]["monitor_convergence"] = False
parameters["krylov_solver"]["report"] = False
parameters["krylov_solver"]["maximum_iterations"] = 50000

def solving_time(A,b, solver):
```

```

U = Function(V)
t0 = time.time()
if len(solver) == 2:
    solve(A, U.vector(), b, solver[0], solver[1]);
else:
    solve(A, U.vector(), b, solver[0]);
t1 = time.time()
return t1-t0

for N in [32, 64, 128, 256, 512, 1024]:

    Ns.append(N)

    mesh = UnitSquare(N, N)
    print " N ", N, " dofs ", mesh.num_vertices()
    V = FunctionSpace(mesh, "Lagrange", 1)
    u = TrialFunction(V)
    v = TestFunction(V)

    f = Expression("sin(x[0]*12) - x[1]")
    a = u*v*dx + inner(grad(u), grad(v))*dx
    L = f*v*dx

    A = assemble(a)
    b = assemble(L)

    t2 = solving_time(A,b, ["lu"])
    print "Time for lu ", t2
    lu_time.append(t2)

    t2 = solving_time(A, b, ["cg"])
    print "Time for cg ", t2
    cg_time.append(t2)

    t2 = solving_time(A, b, ["cg", "ilu"])
    print "Time for cg/ilu ", t2
    cgilu_time.append(t2)

    t2 = solving_time(A, b, ["cg", "amg"])
    print "Time for cg/amg ", t2
    cgamg_time.append(t2)

import pylab

pylab.plot(Ns, lu_time)
pylab.plot(Ns, cg_time)

```

```

pylab.plot(Ns, cgilu_time)
pylab.plot(Ns, cgamg_time)
pylab.xlabel('Unknowns')
pylab.ylabel('Time(sec)')
pylab.legend(["lu", "cg", "cg/ilu", "cg/amg"])
pylab.show()

pylab.loglog(Ns, lu_time)
pylab.loglog(Ns, cg_time)
pylab.loglog(Ns, cgilu_time)
pylab.loglog(Ns, cgamg_time)
pylab.legend(["lu", "cg", "cg/ilu", "cg/amg"])
pylab.savefig('tmp_cpu.pdf')
pylab.show()

```

When we employ iterative methods, we need to specify the convergence criterion. This is often not an easy task. We have the continuous solution u , the discrete solution u_h , and the appropriate discrete solution, u_h^n found by an iterative method at iteration n . Obviously, we may estimate the error as

$$\|u - u_h^n\| \leq \|u - u_h\| + \|u_h - u_h^n\|,$$

and it does make sense that the values of $\|u - u_h\|$ and $\|u_h - u_h^n\|$ are balanced. Still both terms may be hard to estimate in challenging applications. In practice, an appropriate convergence criterion is usually found by trial and error by choosing a stopping criterion based on the residual. Let us therefore consider a concrete example and consider $\|u - u_h^n\|$ as a function of the mesh resolution and a varying convergence criterion.

$\epsilon \setminus N$	64	128	256	512	1024
1.0e-1	1.3e-02 (1.1e-02)	1.4e-02 (3.5e-02)	8.8e-03 (1.4e-01)	3.4e-03 (5.9e-01)	1.1e-02 (2.5e+00)
1.0e-2	1.2e-03 (1.0e-02)	2.0e-03 (3.7e-02)	1.3e-03 (1.5e-01)	3.5e-03 (5.8e-01)	3.7e-04 (2.7e+00)
1.0e-3	3.6e-04 (1.1e-02)	3.1e-04 (3.9e-02)	2.6e-04 (1.6e-01)	2.7e-04 (6.3e-01)	3.7e-04 (2.7e+00)
1.0e-4	3.4e-04 (1.2e-02)	8.5e-05 (4.5e-02)	2.4e-05 (1.8e-01)	3.4e-05 (6.7e-01)	1.4e-05 (2.9e+00)
1.0e-5	3.4e-04 (1.2e-02)	8.4e-05 (4.7e-02)	2.1e-05 (1.9e-01)	5.4e-06 (7.6e-01)	2.8e-06 (3.1e+00)
1.0e-6	3.4e-04 (1.3e-02)	8.4e-05 (5.0e-02)	2.1e-05 (2.1e-01)	5.3e-06 (8.1e-01)	1.3e-06 (3.3e+00)

Table 7.2 The error $\|u - u_h^n\|$ and corresponding CPU time in parenthesis when solving a Poisson problem with homogenous Dirichlet conditions.

Table 7.2 shows the error and the corresponding CPU timings when solving a Poisson problem at various resolutions and convergence criteria. Here, the convergence criteria is chosen as reducing the relative residual, i.e., $\frac{\|r_k\|}{\|r_0\|}$ by the factor ϵ . This convergence criteria is very common, in particular for stationary problems. There are several things to note here. For coarse resolution, $N=64$, the error stagnates somewhere between $1.0e-3$ and $1.0e-4$ and this stagnation marks where an appropriate stopping criteria is. It is however worth noticing that solving it to a criteria that is $1.0e-6$ is actually only about 30% more computationally demanding than $1.0e-3$. This is due to the fact that we have a very efficient method that reduces the error by about a factor 10 per iteration. If we consider the fine resolution, $N=1024$, we see that the stagnation happens later and that we may not even have reached the stagnating point even at $\epsilon = 1.0e-6$. We also notice that the decreasing ϵ in this case only lead to a moderate growth in CPU time. If we look closer at the table, we find that the stagnation point follows a staircase pattern. The code used to generate the table is as follows:

```
from dolfin import *

def boundary(x, on_boundary):
    return on_boundary

parameters["krylov_solver"]["relative_tolerance"] = 1.0e-18
parameters["krylov_solver"]["absolute_tolerance"] = 1.0e-18
parameters["krylov_solver"]["monitor_convergence"] = True
parameters["krylov_solver"]["report"] = True
#parameters["krylov_solver"]["maximum_iterations"] = 50000
epss = [1.0e-1, 1.0e-2, 1.0e-3, 1.0e-4, 1.0e-5, 1.0e-6]
data = {}
Ns = [64, 128, 256, 512, 1024]
#Ns = [8, 16, 32, 64]
for N in Ns:
    for eps in epss:
        parameters["krylov_solver"]["relative_tolerance"] = eps

        mesh = UnitSquareMesh(N, N)
        V = FunctionSpace(mesh, "P", 1)
        u = TrialFunction(V)
        v = TestFunction(V)

        u_ex = Expression("sin(3.14*x[0])*sin(3.14*x[1])", degree=
                           3)
        f = Expression("2*3.14*3.14*sin(3.14*x[0])*sin(3.14*x[1])"
                        , degree=3)
        a = inner(grad(u), grad(v))*dx
```

```

L = f*v*dx

U = Function(V)

A = assemble(a)
b = assemble(L)

bc = DirichletBC(V, u_ex, boundary)
bc.apply(A)
bc.apply(b)

t0 = time()
solve(A, U.vector(), b, "gmres", "amg")
t1 = time()

cpu_time = t1-t0
error_L2 = errornorm(u_ex, U, 'L2', degree_rise=3)
data[(N, eps)] = (error_L2, cpu_time)

for eps in epss:
    for N in Ns:
        D1, D2 = data[(N, eps)]
        print " %3.1e (%3.1e) " % (D1, D2),
        print ""

```

Eigenvalues of the preconditioned system.

It is often interesting to assess the condition number of the preconditioned system, BA . If the preconditioner is a matrix and the size of the system is moderate we may be able to estimate the condition number of BA using NumPy, Matlab or Octave. However, when our preconditioner is an algorithm representing a linear operator, such as in the case of multigrid, then this is not possible. However, as described in [15], eigenvalues may be estimated as a bi-product of the Conjugate Gradient method. Without going into the algorithmic details of the implementation, we mention that this is implemented in the FEniCS module `cbc.block`, see [12]. The following code shows the usage.

```

from dolfin import *
from block.iterative import ConjGrad
from block.algebraic.petsc import ML
from numpy import random

def boundary(x, on_boundary):
    return on_boundary

```

```

class Source(Expression):
    def eval(self, values, x):
        dx = x[0] - 0.5; dy = x[1] - 0.5
        values[0] = 500.0*exp(-(dx*dx + dy*dy)/0.02)

Ns = [8, 16, 32, 64, 128, 256, 512, 1024]
for N in Ns:
    mesh = UnitSquareMesh(N,N)
    V = FunctionSpace(mesh, "CG", 1)

    # Define variational problem
    v = TestFunction(V)
    u = TrialFunction(V)
    f = Source(degree=3)
    a = dot(grad(v), grad(u))*dx
    L = v*f*dx
    bc = DirichletBC(V, Constant(0), boundary)

    # Assemble matrix and vector, create precondition and
    # start vector
    A, b = assemble_system(a,L, bc)
    B = ML(A)
    x = b.copy()
    x[:] = random.random(x.size(0))

    # solve problem and print out eigenvalue estimates.
    Ainv = ConjGrad(A, precondition=B, initial_guess=x, tolerance=
        1e-8, show=2)

    x = Ainv*b
    e = Ainv.eigenvalue_estimates()
    print "N=%d iter=%d K=%.3g" % (N, Ainv.iterations, e[-1]/e
        [0])

```

In this example we see that the condition number increases logarithmic from 1.1 to 2.1 as the N increases from 8 to 1024. The AMG preconditioner has better performance and does not show logarithmic growth. For indefinite symmetric systems, the CGN method provides the means for estimating the condition number, c.f., the `cbc.block` documentation.

7.3.1 Insight from Functional Analysis

In the previous Chapters 5 and 6 we have discussed the well-posedness of the convection-diffusion equations and the Stokes problem. In both cases, the problems were well-posed - meaning that the differential operators as well as their inverse were continuous. However, when we discretize the problems we get matrices where the condition number grows to infinity as the element size goes to zero. This seem to contradict the well-posedness of our discrete problems and may potentially destroy both the accuracy and efficiency of our numerical algorithms. Functional analysis explains this apparent contradiction and explains how the problem is circumvented by preconditioning.

Let us now consider the seeming contradiction in more precise mathematical detail for the Poisson problem with homogeneous Dirichlet conditions: Find u such that

$$-\Delta u = f, \quad \text{in } \Omega, \quad (7.9)$$

$$u = 0, \quad \text{on } \partial\Omega. \quad (7.10)$$

We know from Lax-Milgram's theorem that the weak formulation of this problem: Find $u \in H_0^1$ such that

$$a(u, v) = b(v), \quad \forall v \in H_0^1.$$

where

$$a(u, v) = \int_{\Omega} \nabla u \cdot \nabla v \, dx, \quad (7.11)$$

$$b(v) = \int_{\Omega} f v \, dx, \quad (7.12)$$

is well-posed because

$$a(u, u) \geq \alpha |u|_1^2, \quad \forall u \in H_0^1 \quad (7.13)$$

$$a(u, v) \leq C |u|_1 |v|_{H_0^1} \quad \forall u, v \in H_0^1. \quad (7.14)$$

Here $|\cdot|_1$ denotes the H^1 semi-norm which is known to be a norm on H_0^1 due to Poincare. The well-posedness is in this case stated as

$$|u|_{H_0^1} \leq \frac{1}{\alpha} \|f\|_{H^{-1}}. \quad (7.15)$$

In other words, $-\Delta$ takes a function u in H_0^1 and returns a function $f = -\Delta u$ which is in H^{-1} . We have that $\|f\|_{-1} = \|-\Delta u\|_{-1} \leq C\|u\|_1$. Also, $-\Delta^{-1}$ takes a function f in H^{-1} and returns a function $u = (-\Delta)^{-1}f$ which is in H_0^1 . We have that $\|u\|_1 = \|(-\Delta)^{-1}f\|_1 \leq \frac{1}{\alpha}\|f\|_{-1}$. In fact, in this case $\alpha = C = 1$.

This play with words and symbols may be formalized by using operator norms that are equivalent with matrix norms. Let $B \in \mathbb{R}^{n,m}$ then

$$\|B\|_{\mathcal{L}(\mathbb{R}^m, \mathbb{R}^n)} = \max_{x \in \mathbb{R}^m} \frac{\|Bx\|_{\mathbb{R}^n}}{\|x\|_{\mathbb{R}^m}}$$

Here $\mathcal{L}(\mathbb{R}^m, \mathbb{R}^n)$ denotes the space of all $m \times n$ matrices.

Analogously, we may summarize the mapping properties of $-\Delta$ and $(-\Delta)^{-1}$ in terms of the conditions of Lax-Milgram's theorem as

$$\|-\Delta\|_{\mathcal{L}(H_0^1, H^{-1})} \leq C \quad \text{and} \quad \|(-\Delta)^{-1}\|_{\mathcal{L}(H^{-1}, H_0^1)} \leq \frac{1}{\alpha}. \quad (7.16)$$

where $\mathcal{L}(X, Y)$ denotes the space of bounded linear operators mapping X to Y . In other words, $-\Delta$ is a bounded linear map from H_0^1 to H^{-1} and $(-\Delta)^{-1}$ is a bounded linear map from H^{-1} to H_0^1 . This is a crucial observation in functional analysis that, in contrast to the case of a matrix which is a bounded linear map from \mathbb{R}^n to \mathbb{R}^m , an operator may be map from one space to another.

From Chapter 2 we know that the eigenvalues and eigenvectors of $-\Delta$ with homogeneous Dirichlet conditions on the unit interval in 1D are $\lambda_k = (\pi k)^2$ and $e_k = \sin(\pi k x)$, respectively. Hence the eigenvalues of $-\Delta$ obviously tend to ∞ as k grows to ∞ and similarly the eigenvalues of $(-\Delta)^{-1}$ accumulate at zero as $k \rightarrow \infty$. Hence the spectrum of $-\Delta$ is unbounded and the spectrum of $(-\Delta)^{-1}$ has an accumulation point at zero. Still, the operator $-\Delta$ and its inverse are bounded from a functional analysis point of view, in the sense of (7.18).

Let us for the moment assume that we have access to an operator B with mapping properties that are inverse to that of $A = -\Delta$, i.e.,

$$\|B\|_{\mathcal{L}(H^{-1}, H_0^1)} \quad \text{and} \quad \|B^{-1}\|_{\mathcal{L}(H_0^1, H^{-1})}. \quad (7.17)$$

Then it follows directly that

$$\|BA\|_{\mathcal{L}(H_0^1, H_0^1)} \quad \text{and} \quad \|(BA)^{-1}\|_{\mathcal{L}(H_0^1, H_0^1)}. \quad (7.18)$$

and the condition number

$$\kappa(BA) = \frac{\max_i \lambda_i(BA)}{\min_i \lambda_i(BA)} = \|BA\|_{\mathcal{L}(H_0^1, H_0^1)} \|(BA)^{-1}\|_{\mathcal{L}(H_0^1, H_0^1)}$$

would be bounded. In the discrete case, the mapping property (7.17) translates to the fact that B should be spectrally equivalent with the inverse of A when B and A are both positive.

While the above discussion is mostly just a re-iteration of the concept of spectral equivalence in the discrete case when the PDEs are elliptic, the insight from functional analysis can be powerful for systems of PDEs. Let us consider the Stokes problem from Chapter 6. The problem reads:

$$\mathcal{A} \begin{bmatrix} u \\ p \end{bmatrix} = \begin{bmatrix} -\Delta & -\nabla \\ \nabla \cdot & 0 \end{bmatrix} \begin{bmatrix} u \\ p \end{bmatrix} = \begin{bmatrix} u \\ p \end{bmatrix}$$

As discussed in Chapter 6

$$\mathcal{A} : H_0^1 \times L^2 \rightarrow H^{-1} \times L^2$$

was a bounded linear mapping with a bounded inverse. Therefore, a preconditioner can be constructed as

$$\mathcal{B} = \begin{bmatrix} (-\Delta)^{-1} & 0 \\ 0 & I \end{bmatrix}$$

Clearly

$$\mathcal{B} : H^{-1} \times L^2 \rightarrow H_0^1 \times L^2$$

and is therefore a suitable preconditioner. However, we also notice that \mathcal{A} and \mathcal{B}^{-1} are quite different. \mathcal{A} is indefinite and has positive and negative eigenvalues, while \mathcal{B} is clearly positive. Hence, the operators are not spectrally equivalent. Exercise 7.9 looks deeper into this construction of preconditioners for Stokes problem. A more comprehensive description of this technique can be found in [13].

7.4 Exercises

Exercise 7.1 Estimate ratio of non-zeros per unknown of the stiffness matrix on the unit square with Lagrangian elements of order 1, 2, 3 and 4. Hint: the number of non-zeros can be obtained from the function 'nnz' of a matrix object.

Exercise 7.2 Compute the smallest and largest eigenvalues of the mass matrix and the stiffness matrix in 1D, 2D and 3D. Assume that the condition number is on the form $\kappa \approx Ch^\alpha$, where C and α may depend on the number of dimensions in space. Finally, compute the corresponding condition numbers. Does the condition number have the same dependence on the number of dimensions in space?

Exercise 7.3 Repeat Exercise 7.2 but with Lagrange elements of order 1, 2 and 3. How does the order of the polynomial affect the eigenvalues and condition numbers.

Exercise 7.4 Compute the eigenvalues of the discretized Stokes problem using Taylor-Hood elements. Note that the problem is indefinite and that there are both positive and negative eigenvalues. An appropriate condition number is:

$$\kappa = \frac{\max_i |\lambda_i|}{\min_i |\lambda_i|}$$

where λ_i are the eigenvalues of A . Compute corresponding condition numbers for the Mini and Crouzeix-Raviart elements. Are the condition numbers similar?

Exercise 7.5 Implement the Jacobi iteration for a 1D Poisson problem with homogeneous Dirichlet conditions. Start the iteration with an initial random vector and estimate the number of iterations required to reduce the L_2 norm of the residual with a factor 10^4 . For relevant code see Example 7.3.

Exercise 7.6 Test CG method without preconditioner, with ILU preconditioner and with AMG preconditioner for the Poisson problem in 1D and 2D with homogeneous Dirichlet conditions, with respect to different mesh resolutions. Do some of the iterations suggest spectral equivalence?

Exercise 7.7 Test CG, BiCGStab, GMRES with ILU, AMG, and Jacobi preconditioning for

$$\begin{aligned} -\mu \Delta u + v \nabla u &= f & \text{in } \Omega \\ u &= 0 & \text{on } \partial\Omega \end{aligned}$$

Where Ω is the unit square, $v = c \sin(7x)$, and c varies as 1, 10, 100, 1000, 10000 and the mesh resolution h varies as $1/8, 1/16, 1/32, 1/64$. You may assume homogeneous Dirichlet conditions.

Exercise 7.8 The following code snippet shows the assembly of the matrix and preconditioner for a Stokes problem:

```
a = inner(grad(u), grad(v))*dx + div(v)*p*dx + q*div(u)*dx
L = inner(f, v)*dx

# Form for use in constructing preconditioner matrix
b = inner(grad(u), grad(v))*dx + p*q*dx

# Assemble system
A, bb = assemble_system(a, L, bcs)

# Assemble preconditioner system
P, btmp = assemble_system(b, L, bcs)

# Create Krylov solver and AMG preconditioner
solver = KrylovSolver("tfqmr", "amg")

# Associate operator (A) and preconditioner matrix (P)
solver.set_operators(A, P)

# Solve
U = Function(W)
solver.solve(U.vector(), bb)
```

Here, "tfqmr" is a variant of the Minimal residual method and "amg" is an algebraic multigrid implementation in HYPRE. Test, by varying the mesh resolution, whether the code produces an order-optimal preconditioner. HINT: You might want to change the "parameters" as done in Example 7.3:

```
# Create Krylov solver and AMG preconditioner
solver = KrylovSolver("tfqmr", "amg")
solver.parameters["relative_tolerance"] = 1.0e-8
solver.parameters["absolute_tolerance"] = 1.0e-8
solver.parameters["monitor_convergence"] = True
solver.parameters["report"] = True
solver.parameters["maximum_iterations"] = 50000
```

Exercise 7.9 Consider the mixed formulation of linear elasticity that is appropriate when λ is large compared to μ . That is,

```
a = inner(grad(u), grad(v))*dx + div(v)*p*dx + q*div(u)*dx - 1
                                     /lam*p*q*dx
L = inner(f, v)*dx
```

Create two preconditioners:

```
b1 = inner(grad(u), grad(v))*dx + p*q*dx  
b2 = inner(grad(u), grad(v))*dx + 1/lam*p*q*dx
```

Compare the efficiency of the different preconditioners when increasing the resolution and when $\lambda \rightarrow \infty$. Can you explain why the first preconditioner is the best?

Chapter 8

Linear elasticity and singular problems

8.1 Introduction

Let us consider an elastic body Ω_0 that is being deformed under a load to become Ω . the deformation χ of a body in the undeformed state Ω_0 to deformed state Ω . A point in the body has then moved

$$u = x - X, \quad (8.1)$$

by definition this is *displacement field*. An illustration is shown in Figure 8.1.

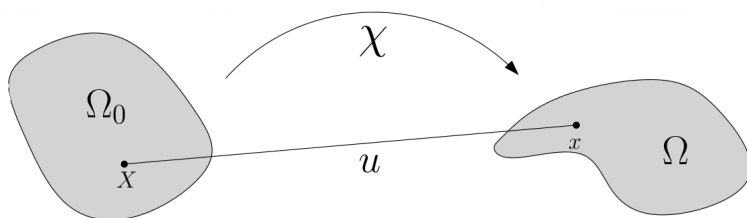


Fig. 8.1 Deforming body and displacement vector u .

Here, the domain $\Omega_0 \subset \mathbb{R}^3$. From continuum mechanics, the elastic deformation is modelled by the stress tensor σ which is a symmetric 3×3 tensor. In equilibrium (i.e. no acceleration terms) the Newton's second law states the balance of forces as:

$$\begin{aligned}\operatorname{div} \sigma &= f, & \text{in } \Omega, \\ \sigma \cdot n &= g, & \text{on } \partial\Omega,\end{aligned}$$

where f and g are body and surface forces, respectively and n is the outward normal vector.

For small deformations of an isotropic media, Hooke's law is a good approximation. Hooke's law states that

$$\sigma = 2\mu\epsilon(u) + \lambda \operatorname{tr}(\epsilon(u))\delta.$$

Here, $\epsilon(u)$ is the strain tensor or the symmetric gradient:

$$\epsilon(u) = \frac{1}{2}(\nabla u + (\nabla u)^T),$$

μ and λ are the Lamé constants, tr is the trace operator (the sum of the diagonal matrix entries), u is the displacement, and

$$\delta = \begin{bmatrix} 1 & 0 & 0 \\ 0 & 1 & 0 \\ 0 & 0 & 1 \end{bmatrix}.$$

From Newton's second law and Hooke's law we arrive directly at the equation of linear elasticity:

$$-2\mu(\nabla \cdot \epsilon(u)) - \lambda \nabla(\nabla \cdot u) = f. \quad (8.2)$$

The equation of linear elasticity (8.2) is an elliptic equation, but there are crucial differences between this equation and a standard elliptic equation like $-\Delta u = f$. These differences often cause problems in a numerical setting. To explain the numerical issues we will here focus on the differences between the three operator:

1. $-\Delta = \nabla \cdot \nabla = \operatorname{div} \operatorname{grad}$,
2. $\nabla \cdot \epsilon = \nabla \cdot (\frac{1}{2}(\nabla + (\nabla^T)))$,
3. $\nabla \cdot \operatorname{tr} \epsilon = \nabla \nabla \cdot = \operatorname{grad} \operatorname{div}$.

In particular, the differences between the operators in 1. and 2. is that $\nabla \cdot \epsilon$ has a larger kernel than $-\Delta$. The kernel consists of rigid motions and this leads to the usage of one of Korn's lemmas. This is the subject of Section 8.2. The kernel of the operators $\operatorname{grad} \operatorname{div}$ and $\operatorname{div} \operatorname{grad}$ are also different but here in fact the kernel of $\operatorname{grad} \operatorname{div}$ is infinite dimensional and this has different

consequences for the numerical algorithms which not necessarily pick up this kernel at all. This is discussed in Section 8.3.

8.2 The operator $\nabla \cdot \epsilon$ and rigid motions

The challenge with the handling of the $\nabla \cdot \epsilon$ operator is the handling of the singularity in the case of pure Neumann conditions. Let us therefore start with the simpler problem of the Poisson problem with Neumann conditions, i.e.,

$$-\Delta u = f, \quad \text{in } \Omega, \quad (8.3)$$

$$\frac{\partial u}{\partial n} = g, \quad \text{on } \partial\Omega. \quad (8.4)$$

It is easy to see that this problem is singular: Let u be a solution of the above equation, then $u + C$ with $C \in \mathbb{R}$ is also a solution because $-\Delta u = \Delta(u + C) = f$ and $\frac{\partial u}{\partial n} = \frac{\partial(u+C)}{\partial n} = g$. Hence, the solution is only determined up to a constant. This means that the kernel is 1-dimensional.

A proper formulation of the above problem can be obtained by using the method of Lagrange multipliers to fixate the element of the 1-dimensional kernel. The following weak formulation is well-posed: Find $u \in H^1$ and $\lambda \in \mathbb{R}$ such that

$$a(u, v) + b(\lambda, v) = f(v) \quad \forall v \in H^1 \quad (8.5)$$

$$b(u, \gamma) = 0, \quad \forall \gamma \in \mathbb{R}. \quad (8.6)$$

Here,

$$a(u, v) = (\nabla u, \nabla v), \quad (8.7)$$

$$b(\lambda, v) = (\lambda, v), \quad (8.8)$$

$$f(v) = (f, v) + \int_{\partial\Omega} g v ds. \quad (8.9)$$

Hence, the method of Lagrange multipliers turns the original problem into a saddle problem similar that in Chapter 6. However, in this case the Brezzi conditions are easily verified. We remark however that this formulation makes the problem indefinite rather than positive definite and for this reason alternative techniques such as pin-pointing is often used instead. We will not avocate this approach as it often causes numerical problems. Instead, we include a

code example that demonstrate how this problem can be implemented with the method of Lagrange multipliers in FEniCS.

```

from dolfin import *

mesh = UnitSquareMesh(64, 64)

# Build function space with Lagrange multiplier
P1 = FiniteElement("Lagrange", mesh.ufl_cell(), 1)
R = FiniteElement("Real", mesh.ufl_cell(), 0)
W = FunctionSpace(mesh, P1 * R)

# Define variational problem
(u, c) = TrialFunction(W)
(v, d) = TestFunctions(W)
f = Expression("10*exp(-(pow(x[0] - 0.5, 2) + pow(x[1] - 0.5, 2)) / 0.02)", degree=2)
g = Expression("-sin(5*x[0])", degree=2)
a = (inner(grad(u), grad(v)) + c*v + u*d)*dx
L = f*v*dx + g*v*ds

# Compute solution
w = Function(W)
solve(a == L, w)
(u, c) = w.split()

# Plot solution
plot(u, interactive=True)

```

The kernel of the ϵ operator is the space of rigid motions, RM. The space consists of translations and rotations. Rigid motions are on the following form in 2D and 3D:

$$\text{RM}_{2D} = \begin{bmatrix} a_0 \\ a_1 \end{bmatrix} + a_2 \begin{bmatrix} -y \\ x \end{bmatrix}, \quad (8.10)$$

$$\text{RM}_{3D} = \begin{bmatrix} a_0 \\ a_1 \\ a_2 \end{bmatrix} + \begin{bmatrix} 0 & a_3 & a_4 \\ -a_3 & 0 & a_5 \\ -a_4 & -a_5 & 0 \end{bmatrix} \begin{bmatrix} x \\ y \\ z \end{bmatrix}. \quad (8.11)$$

Hence, the kernel in 2D is three-dimensional and may be expressed as above in terms of the degrees of freedom (a_0, a_1, a_2) whereas the kernel in 3D is six-dimensional (a_0, \dots, a_5) .

The Korn's lemmas states suitable conditions for solvability. Here, we include two of the three inequalities typically listed.

- The first lemma: For all $u \in H^1 \setminus \text{RM}$ we have that $\|\epsilon(u)\| \geq C\|u\|_1$.

- The second lemma: For all $u \in H_0^1$ we have that $\|\epsilon(u)\| \geq C\|u\|_1$.

These lemmas should be compared with the Poincaré's lemma and the equivalence of the $|\cdot|_1$ and $\|\cdot\|_1$ norms. The second lemma states that when we have homogenous Dirichlet conditions we obtain a well-posed problem in a similar manner as for a standard elliptic problem. This case is often called fully-clamped conditions. For the Neumann problem, however, coersivity is not obtained unless we remove the complete set of rigid motions for the function space used for trial and test functions. Removing the rigid motions is most easily done by using the method of Lagrange multipliers.

Let us now consider a weak formulation of the linear elasticity problem and describe how to implement it in FEniCS. For now we consider the case where λ and μ are of comparable magnitude. In the next section we consider the case where $\lambda \gg \mu$. The weak formulation of the linear elasticity problem is: Find $u \in H^1$ and $r \in \text{RM}$ such that

$$a(u, v) + b(r, v) = f(v), \quad \forall v \in H^1, \quad (8.12)$$

$$b(s, u) = 0, \quad \forall s \in \text{RM}. \quad (8.13)$$

Here,

$$a(u, v) = \mu(\epsilon(u), \epsilon(v)) + \lambda(\text{div } u, \text{div } v) \quad (8.14)$$

$$b(r, v) = (r, v), \quad (8.15)$$

$$f(v) = (f, v) + \int_{\partial\Omega} g v ds. \quad (8.16)$$

As we know from Chapter 6, this is a saddle point problem and we need to comply with the Brezzi conditions. Verifying these conditions are left as Exercise 8.4.

O

ur brain and spinal cord is floating in a water like fluid called the cerebrospinal fluid. While the purpose of this fluid is not fully known, it is known that the pressure in the fluid oscillates with about 5-10 mmHg during a cardiac cycle which is approximately one second, c.f., e.g., [5]. The Youngs' modulus has been estimated 16 kPa and 1 mmHg \approx 133 Pa, c.f., e.g., [16]. To compute the deformation of the brain during a cardiac cycle we consider solve the linear elasticity problem with Neumann condtions set as pressure of 1 mm Hg and ... The following code shows the implmentation in FEniCS. The mesh of the

brain was in this case obtained from a T1 magnetic resonance image and segmentation was performed by using FreeSurfer.

```

from fenics import *

mesh = Mesh('mesh/res32.xdmf') # mm

plot(mesh, interactive=True)

# Since the mesh is in mm pressure units in pascal must be
# scaled by alpha = (1e6)**(-1)
alpha = (1e6)**(-1)

# Mark boundaries
class Neumann_boundary(SubDomain):
    def inside(self, x, on_boundary):
        return on_boundary

mf = FacetFunction("size_t", mesh)
mf.set_all(0)

Neumann_boundary().mark(mf, 1)
ds = ds[mf]

# Continuum mechanics
E = 16*1e3 *alpha
nu = 0.25
mu, lambda_ = Constant(E/(2*(1 + nu))), Constant(E*nu/((1 + nu)
                                                    *(1 - 2*nu)))
epsilon = lambda_ u: sym(grad(u))

p_outside = 133 *alpha
n = FacetNormal(mesh)
f = Constant((0, 0, 0))

V = VectorFunctionSpace(mesh, "Lagrange", 1)

# ----- Handle Neumann-problem ----- #
R = FunctionSpace(mesh, 'R', 0) # space for one
                                Lagrange multiplier
M = MixedFunctionSpace([R]*6)   # space for all
                                multipliers
W = MixedFunctionSpace([V, M])
u, rs = TrialFunctions(W)
v, ss = TestFunctions(W)

# Establish a basis for the nullspace of RM
e0 = Constant((1, 0, 0)) # translations

```

```

e1 = Constant((0, 1, 0))
e2 = Constant((0, 0, 1))

e3 = Expression((-x[1]', 'x[0]', '0')) # rotations
e4 = Expression((-x[2]', '0', 'x[0]'))
e5 = Expression(('0', '-x[2]', 'x[1]'))
basis_vectors = [e0, e1, e2, e3, e4, e5]

a = 2*mu*inner(epsilon(u),epsilon(v))*dx + lambda_*inner(div(u
),div(v))*dx
L = inner(f, v)*dx + p_outside*inner(n,v)*ds(1)

# Lagrange multipliers contrib to a
for i, e in enumerate(basis_vectors):
    r = rs[i]
    s = ss[i]
    a += r*inner(v, e)*dx + s*inner(u, e)*dx

# ----- #

# Assemble the system
A = PETScMatrix()
b = PETScVector()
assemble_system(a, L, A_tensor=A, b_tensor=b)

# Solve
uh = Function(W)
solver = PETScLUSolver('mumps') # NOTE: we use direct solver
                                   for simplicity
solver.set_operator(A)
solver.solve(uh.vector(), b)

# Split displacement and multipliers. Plot
u, ls = uh.split(deepcopy=True)
plot(u, mode='displacement', title='Neumann_displacement',
      interactive=True)

file = File('deformed_brain.pvd')
file << u

```

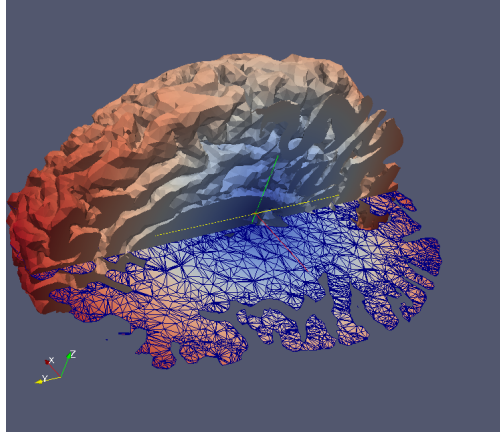


Fig. 8.2 Deformation of the human brain during a cardiac cycle.

8.3 Locking

The locking phenomena has nothing to do with the problem related to the rigid motions studied in the previous section. Therefore, we consider locking in the simplest case possible where we have homogenous Dirichlet conditions. In this case the elasticity equation can be reduced to

$$\begin{aligned} -\mu\Delta u - (\mu + \lambda)\nabla\nabla \cdot u &= f, & \text{in } \Omega, \\ u &= 0, & \text{on } \partial\Omega. \end{aligned}$$

The weak formulation of the problem then becomes: Find $u \in H_0^1$ such that

$$a(u, v) = f(v), \quad \forall v \in H_0^1,$$

where

$$a(u, v) = \mu(\nabla u, \nabla v) + (\mu + \lambda)(\nabla \cdot u, \nabla \cdot v), \quad (8.17)$$

$$f(v) = (f, v). \quad (8.18)$$

The phenomenon locking is a purely numerical artifact that arises when $\lambda \gg \mu$. Roughly speaking, approximating ∇ and $\nabla \cdot$ require different methods. While vertex based approximations work fine for ∇ , edge based methods are more

natural for $\nabla \cdot$ since this operator relates directly to the flux through the element edges.

For smooth functions, it can be verified directly that

$$\Delta = \nabla \cdot \nabla = \nabla \nabla \cdot + \nabla \times \nabla \times$$

where $\nabla \times$ is the curl operator. Hence in H_0^1 we have

$$(\nabla u, \nabla v) = (\nabla \cdot u, \nabla \cdot v) + (\nabla \times u, \nabla \times v).$$

Furthermore, it is well known (the Helmholtz decomposition theorem) that any field in L^2 or H^1 can be decomposed into a the gradient of a scalar potential (irrotational, curl-free vector field) and the curl of scalar (a solenoidal, divergence-free vector field). That is,

$$u = \nabla \phi + \nabla \times \psi,$$

where ϕ and ψ are scalar fields that can be determined. Furthermore,

$$\nabla \cdot \nabla \times u = 0, \tag{8.19}$$

$$\nabla \times \nabla \cdot u = 0. \tag{8.20}$$

This means that

$$\nabla \nabla \cdot u = \begin{cases} \Delta u & \text{if } u \text{ is a gradient} \\ 0 & \text{if } u \text{ is a curl} \end{cases}$$

As the material becomes incompressible, when $\lambda \rightarrow \infty$ the gradient part is being locked and ϕ tends to zero. However, the curl represented by ψ remains unaffected. Vertex based finite elements such as Lagrange are poor at distinguishing between gradients and curls and tend to lock the complete solution. Exercise 8.5 investigates this phenomena numerically.

To avoid locking it is common to introduce a the quantity solid pressure, $p = (\mu + \lambda) \nabla \cdot u$. Introducing this as a separate unknown into the system we obtain the equations:

$$\begin{aligned} -\mu \Delta u - \nabla p &= f, \\ \nabla \cdot u - \frac{1}{\mu + \lambda} p &= 0. \end{aligned}$$

This system of equations is similar to the Stokes problem. Hence, we may formulate a weak problems as follows. Find $u \in H_0^1$ and $p \in L^2$ such that

$$a(u, v) + b(p, v) = f(v) \forall v \in H^1 \quad (8.21)$$

$$b(u, q) - c(p, q) = 0, \forall q \in \mathbb{R}. \quad (8.22)$$

Here,

$$a(u, v) = (\nabla u, \nabla v), \quad (8.23)$$

$$b(p, v) = (\nabla p, v), \quad (8.24)$$

$$c(p, q) = \frac{1}{\mu + \lambda}(p, q) \quad (8.25)$$

$$f(v) = (f, v). \quad (8.26)$$

The case when $\lambda \rightarrow \infty$ then represents the Stokes problem as $\frac{1}{\mu + \lambda} \rightarrow 0$. Hence, for this problem we know that stable discretizations can be obtained as long as we have Stokes-stable elements like for instance Taylor–Hood. We also remark that Stokes-stable elements handle any μ, λ because the $-c(p, q)$ is a negative term that only stabilize. In fact, this problem is identical to the proposed penalty method that was discussed for the Stokes problem.

Exercise 8.1 Show that the inner product of a symmetric matrix A and matrix B equals the inner product of A and the symmetric part of B , i.e., that $A : B = A : B_S$, where $B_S = \frac{1}{2}(B + B^T)$.

Exercise 8.2 Show that the term $\operatorname{div} \epsilon(u)$ in a weak setting may be written as $(\epsilon(u), \epsilon(v))$. Use the result of Exercise 8.1.

Exercise 8.3 Show that the Brezzi conditions (6.15-6.18) for the singular problem of homogenous Neumann conditions for the Poisson problem (8.5)–(8.9). Hint: use the following version of Poincaré’s lemma:

$$\|u - \bar{u}\|_0 \leq C \|\nabla u\|_0, \quad \forall u \in H^1.$$

Here, $\bar{u} = \frac{1}{|\Omega|} \int_{\Omega} u dx$. As always, the inf-sup condition is challenging, but notice that

$$\sup_{u \in V_h} \frac{b(u, q)}{\|u\|_{V_h}} \geq \frac{b(\bar{u}, q)}{\|\bar{u}\|_{V_h}}.$$

Exercise 8.4 Show that three of Brezzi conditions (6.15-6.17) for problem linear elasticity problem with pure Neumann conditions (8.12)–(8.13) are valid. Hint: use Korn’s lemma for the coersivity. As always, the inf-sup condition is challenging and we refer to [10].

Exercise 8.5 We will consider the topic 'locking'. Consider the following equation on the domain $\Omega = (0, 1)^2$:

$$-\mu\Delta u - \lambda\nabla\nabla \cdot u = f \text{ in } \Omega, \quad (8.27)$$

$$u = u_{\text{analytical}} \text{ on } \partial\Omega \quad (8.28)$$

where $u_{\text{analytical}} = (\frac{\partial\phi}{\partial y}, -\frac{\partial\phi}{\partial x})$ and $\phi = \sin(\pi xy)$. Here, by construction, $\nabla \cdot u_{\text{analytical}} = 0$.

- a) Derive an expression for f . Check that the expression is independent of λ .
- b) Compute the numerical error for $\lambda = 1, 100, 10000$ at $h = 8, 16, 32, 64$ for polynomial order both 1 and 2.
- c) Compute the order of convergence for different λ . Is locking occurring?

Chapter 9

Alternative Formulations

9.1 Introduction

Most commonly, the basis for finite element methods has been the weak formulation as discussed in the previous chapters. But, with the introduction of neural networks and physics-informed networks, alternative formulations based on least square method principles have been made popular. Such formulations have also been studied earlier, but has in general received little attention as compared with standard weak formulations. In this chapter we will therefore discuss different ways of formulating PDE problems. Let us for simplicity discuss elliptic problems with Dirichlet boundary conditions of the form: Find $u \in C^2(\Omega)$ given $f \in C^0(\Omega)$ of the form

$$-\Delta u = f \quad \text{in } \Omega, \quad (9.1)$$

$$u = g \quad \text{on } \Omega. \quad (9.2)$$

The weak formulation: Find $u \in H_g^1(\Omega)$, given $f \in H^{-1}(\Omega)$ such that

$$\int_{\Omega} \nabla u \cdot \nabla v \, dx = \int_{\Omega} f v \, dx, \quad \forall v \in H_0^1(\Omega), \quad (9.3)$$

follows directly from Gauss-Green's lemma, as we saw in Chapter 4. We will refer to this formulation as the *primal formulation*.

The weak formulation may alternatively be derived from energy considerations. That is, consider the energy functional,

$$E(v, f) = \int_{\Omega} \frac{1}{2} (\nabla v)^2 - f v \, dx. \quad (9.4)$$

The solution of (9.3) can equivalently be written as the minimizer of this energy functional. That is,

$$u = \arg \min_{v \in H_g^1(\Omega)} E(v, f). \quad (9.5)$$

KAM: use u, v, w_i such that both u and v can be expressed as a linear combination of w_i

To see the relationship between the two formulations we need to be able to differentiate the functional E with respect to functions v . Assume therefore that $H_g^1(\Omega)$ can be spanned by a basis $\{v_i\}_{i=1}^{\infty}$. Then a function can be expressed as $u = \sum_i u_i v_i$ and we notice directly that

$$\frac{\partial u}{\partial u_i} = v_i. \quad (9.6)$$

Hence,

$$\frac{\partial E}{\partial u_i} = \int_{\Omega} \nabla u \cdot \nabla v_i - f v_i \, dx. \quad (9.7)$$

Furthermore, clearly $E(v, f)$ is minimized when the derivative is zero, i.e.

$$\frac{\partial E}{\partial u_i} = \int_{\Omega} \nabla u \cdot \nabla v_i - f v_i \, dx = 0. \quad (9.8)$$

which corresponds to the weak formulation.

9.2 Least square formulation of primal formulation

An alternative "energy"-like functional, based on least square principles that could be minimized would be

$$E_{LS} = \| -\Delta u - f \|_{L^2(\Omega)} \quad (9.9)$$

Again, we seek to find the minimizer

$$u = \arg \min_{v \in ?} E_{LS}(v, f). \quad (9.10)$$

We differentiate in order to find that

$$\frac{\partial E_{LS}}{\partial u_i} = \int_{\Omega} \frac{\partial}{\partial u_i} (-\Delta u - f)^2 dx = \quad (9.11)$$

$$2 \int_{\Omega} (-\Delta u - f)(-\Delta v_i) dx \quad (9.12)$$

By applying Gauss-Green's lemma again we may again derive a corresponding strong formulation: Find u such that

$$\Delta^2 u = -\Delta f \quad \text{in } \Omega, \quad (9.13)$$

$$u = g \quad \text{on } \partial\Omega, \quad (9.14)$$

$$-\Delta u = f \quad \text{on } \partial\Omega. \quad (9.15)$$

We refer (9.11) and (9.13) as the weak and strong formulation of the least square formulation of the primal problem. We notice that both formulations requires more regularity than the standard weak formulation of the primal problem. In fact (9.13) requires $u \in C^4(\Omega)$ whereas (9.11) is naturally posed in $H_g^2(\Omega)$.

9.3 The Mixed formulation

To reduce the number of derivatives on the solution, a common trick is to split the original second order equation into two equations of first order. That is, we notice that

$$-\Delta u = f \quad (9.16)$$

may be alternatively written as

$$\psi = \nabla u, \quad (9.17)$$

$$\nabla \cdot \psi = f. \quad (9.18)$$

That is, inserting (9.17) into the (9.18) directly gives (9.16). Here, we notice that ψ is a vector field while u is a scalar field.

Also this problem may be phrased as a minimization problem, although a constrained minimization problem. Let the energy be

$$E_M(\psi) = \int_{\omega} \frac{1}{2} \psi^2 dx$$

The the solution is

$$u = \arg \min_{\nabla \cdot \psi = f} E_M(v). \quad (9.19)$$

The constraint $\nabla \cdot v = f$ may be enforced using a Lagrange multiplier. Then the functional becomes

$$L(v, \lambda, f) = \int_{\Omega} v^2 dx + \int_{\Omega} (\nabla \cdot v = g) \lambda dx$$

and

$$u, \mu = \arg \min_v \arg \max_{\lambda} L(v, \lambda, f). \quad (9.20)$$

Again, we may differentiate (with respect to both v and the Lagrange multiplier λ to find the extremal points of L as

$$\frac{\partial L(u, \lambda)}{\partial v} = \int_{\Omega} v^2 dx + \int_{\Omega} (\nabla \cdot v = g) \lambda dx \quad (9.21)$$

Index

Richardson iteration, 74
Richardson preconditioner, 80

Spectral equivalence, 81

References

1. M. S. ALNÆS AND K.-A. MARDAL, *Syfi and sfc: Symbolic finite elements and form compilation*, Automated Solution of Differential Equations by the Finite Element Method: The FEniCS Book, (2012), pp. 273–282.
2. D. BRAESS, *Finite elements: Theory, fast solvers, and applications in solid mechanics*, Cambridge University Press, 2007.
3. S. C. BRENNER AND R. SCOTT, *The mathematical theory of finite element methods*, vol. 15, Springer Science & Business Media, 2008.
4. P. G. CIARLET, *The finite element method for elliptic problems*, SIAM, 2002.
5. P. K. EIDE, *The correlation between pulsatile intracranial pressure and indices of intracranial pressure-volume reserve capacity: results from ventricular infusion testing*, Journal of neurosurgery, 125 (2016), pp. 1493–1503.
6. H. C. ELMAN, D. SILVESTER, AND A. WATHEN, *Finite elements and fast iterative solvers: with applications in incompressible fluid dynamics*, Oxford University Press, 2014.
7. L. C. EVANS, *Partial differential equations*, vol. 19, American Mathematical Society, 2022.
8. R. C. KIRBY, *Fiat: numerical construction of finite element basis functions*, Automated Solution of Differential Equations by the Finite Element Method: The FEniCS Book, (2012), pp. 247–255.
9. R. C. KIRBY AND K.-A. MARDAL, *Constructing general reference finite elements*, in Automated Solution of Differential Equations by the Finite Element Method: The FEniCS Book, Springer, 2012, pp. 121–132.
10. M. KUCHTA, K.-A. MARDAL, AND M. MORTENSEN, *On the singular neumann problem in linear elasticity*, arXiv preprint arXiv:1609.09425, (2016).
11. A. LOGG, K.-A. MARDAL, AND G. WELLS, *Automated solution of differential equations by the finite element method: The FEniCS book*, vol. 84, Springer Science & Business Media, 2012.
12. K.-A. MARDAL AND J. B. HAGA, *Block preconditioning of systems of pdes*, Automated Solution of Differential Equations by the Finite Element Method, (2012), pp. 643–655.

13. K.-A. MARDAL AND R. WINTHER, *Preconditioning discretizations of systems of partial differential equations*, Numerical Linear Algebra with Applications, 18 (2011), pp. 1–40.
14. A. QUARTERONI AND A. VALLI, *Numerical approximation of partial differential equations*, vol. 23, Springer Science & Business Media, 2008.
15. Y. SAAD, *Iterative methods for sparse linear systems*, SIAM, 2003.
16. K. H. STØVERUD, M. ALNÆS, H. P. LANGTANGEN, V. HAUGHTON, AND K.-A. MARDAL, *Poro-elastic modeling of syringomyelia—a systematic study of the effects of pia mater, central canal, median fissure, white and gray matter on pressure wave propagation and fluid movement within the cervical spinal cord*, Computer methods in biomechanics and biomedical engineering, 19 (2016), pp. 686–698.